Journal of Materials Chemistry B

Accepted Manuscript

ROYAL SOCIETY OF CHEMISTRY

www.rsc.org/materialsB

Insulating and Semiconducting Polymeric Free-Standing Nanomembranes with Biomedical Applications

Maria M. Pérez-Madrigal,[1,2,*] Elaine Armelin,[1,2] Jordi Puiggalí[1,2] and Carlos Alemán[1,2,*]

[1] *Departament d'Enginyeria Química, ETSEIB, Universitat Politècnica de Catalunya, Avda. Diagonal 647, Barcelona E-08028, Spain*

[2] *Center for Research in Nano-Engineering, Universitat Politècnica de Catalunya, Campus Sud, Edifici C', C/Pasqual i Vila s/n, Barcelona E-08028, Spain*

[*] m.mar.perez@upc.edu and carlos.aleman@upc.edu

ABSTRACT

In recent decades, polymers have experienced a radical evolution: from being used as inexpensive materials in the manufacturing of simple appliances to be designed as nanostructured devices with important applications in many leading fields, such as biomedicine at the nanoscale. Within this context, polymeric free-standing nanomembranes –self-supported quasi-2D structures with a thickness ranging from ~10 to a few hundred of nanometers and an aspect ratio of size and thickness greater than 10^6– are emerging as versatile elements for applications as varied as overlapping therapy, burn wound infections treatment, antimicrobial platforms, scaffolds for tissue engineering, drug-loading and delivery systems, biosensors, etc. Although at first, a little over a decade ago, materials for the fabrication of free-standing nanosheets were limited to biopolymers and insulating polymers, which were biodegradable, during the last five years, the use of electroactive conducting polymers has been attracting much attention because of their extraordinary advantages in the biomedical field. In this context, a systematic review of current research on polymeric free-standing nanomembranes for biomedical applications is presented. Moreover, further discussion on the future developments of some of these exciting areas of study and their principal challenges is presented in the conclusions section.

Keywords: Biodegradable polymers; Conducting polymers; Polysaccharides; Self-supported films; Ultra-thin films

1. Introduction

Over the past decades, biomaterials science has been increasingly evolving into a more interdisciplinary field combining elements of medicine, chemistry, biology, engineering and materials science. Recently, nanotechnological concepts and procedures have also been applied to obtain and improve devices with very different applications in biomedicine and biotechnology.[1-3] Specifically, there is a growing interest in the fabrication of nanomembranes (also known as ultra-thin films or nanosheets) since their distinctive features make them suitable for designing sensors,[4,5] nanobiological reactors,[6] biomotors,[7] biointerfaces for cellular matrices,[8] antimicrobial surfaces,[9,10] or drug release devices.[11,12] In practice, the term *nanomembrane* refers to quasi-2D structures with macroscopic surface area and thickness values ranging from 10 to a few hundreds of nm. A few years ago, Kunitake *et al.*[13], pioneers in this field, coined the term "*giant nanomembrane*" to denote self-supporting (namely, free-standing) membranes with thickness from 1 to 100 nm and an aspect ratio of size and thickness greater than 10^6. Such a high aspect ratio facilitates the handling of these nanomembranes, while the self-supporting property, which enables the nanosheet to be removed from its supporting substrate retaining the mechanical integrity, is required to physically separate two spaces. Besides, free-standing nanomenbranes (hereafter denoted FsNM) are characterized by other special properties, such as low weight, high flexibility, robustness, and, in some cases, transparency.[14]

Research on FsNM for biomedical applications started less than a decade ago when it was proved that ultra-thin sheets prepared using biodegradable and biocompatible polyesters and polysaccharides exhibited excellent mechanical properties and adhesion strength. Rapidly, this led to a considerable interest in these nanosheets as novel substrates/biointerfaces to promote cell adhesion, migration, proliferation and

differentiation. More recently, FsNM have been used for different therapeutic uses, as for example treatment of microbial infections, control of cell adhesion and repair of tissue defects. In this review, we discuss the most representative examples of FsNM made of insulating and electrochemically inactive polymers for advanced biomedical applications. After this, we present the very recent achievements in the application of electroactive conducting polymers (ECP) in what we call the "*second generation of FsNM*", which incorporate electrochemical and electrical functionalities to biodegradation and biocompatibility. Before of such discussion, brief explanations about both the different strategies that can be used to fabricate FsNM and the main concepts of ECPs are provided.

2. Preparation of Free-Standing Nanomembranes

Typically, FsNM are produced by depositing nanofilms on solid substrates, or via the fluid-fluid or liquid-air interfaces. In addition, some other approaches, including layer-by-layer (LbL) assembly,[15-17] Langmuir-Blodgett transfer (LB),[18] spin-coating,[19] electrophoretic deposition[20] and cross-linking of self-assembled monolayers (SAM) techniques,[21] also often are employed. These methods differ in two general aspects: (1) the degree of control over the final FsNM thickness, composition and stability; and (2) the step in which the nanomembrane is removed, transferred or extracted from the solid surface or the fluid-fluid interface.[22]

In the LbL technique, which was developed by Decher *et al.*[15-17] in the early 1990s, the formation of the FsNM is achieved by depositing on a solid surface alternating layers of oppositely charged materials (Figure 1a), such as polyions, metals, nanoparticles, ceramics or biological molecules. Accordingly, FsNM stability arises from primary or secondary interactions between those layers. This approach stands out because of its

simplicity and the high degree of control over the FsNM thickness. Furthermore, the precise guidance exerted over the chemical composition of the layers results in a tremendous versatility when designing FsNM.[23] Regarding the SAM technique, Stroock *et al.*[21] extensively described the synthesis of polymeric FsNM with 10-15 nm in thickness and well-defined lateral size and shape.

On the other hand, spin-coating (Figure 1b) is another interesting approach that allows the preparation of single- or multi-layered FsNM in a few steps. In this case, the optimization of the spin-coating parameters (*e.g.* spinning speed and time, and the solution concentration) leads to ultra-thin films with controlled features, thickness and homogeneity. In this procedure, which seems to be the most versatile and easy-going, the liquid polymeric solution is spin-coated onto a solid substrate previously coated with a sacrificial layer. Hence, by dissolving the sacrificial layer in an appropriated solvent, the FsNM is detached from the substrate and released into a liquid environment where it can be then easily handled with syringes or pipettes. Most of the FsNM described in this review were fabricated using a combination of both the LbL assembly and spin-coating procedures.

3. Electroactive Conducting Polymers

Electroactive conducting polymers (ECP) are widely known as electrochemically active organic semiconducting materials. These polymers are special in that they consist of long conjugated polymeric chains that present alternation of double and single-bonded sp^2 hybridized atoms. This conjugation, which is described in terms of electronic wave functions that are delocalized over the entire chain, allows charge mobility along the polymer backbone and between adjacent chains, thus endowing the polymer with semiconductive and electrochemical properties.[24-26] Although the band structure of ECP

is similar to that of inorganic semiconductors, they also exhibit some of the attractive properties associated with conventional polymers (*i.e.* electrically insulating polymers), such as ease of synthesis and flexibility in processing. However, the mechanical stability of ECP is typically lower than that of both inorganic semiconductors and conventional polymers.

The doping process converts neutral ECP into semiconductive. In this process the ECP is oxidized (p-doping) or reduced (n-doping) and, as a result, positive or negative charge carriers, respectively, are introduced onto the backbone. Backbone charge carriers, which typically consists of charged polarons (*i.e.* radical cations or anions) or bipolarons (*i.e.* dications or dianions),[27] are accompanied by counter ions with opposite charges that are entrapped into the polymer matrix to maintain electrical neutrality. Simultaneously, the band structure of the ECP is modified to accommodate the formation of polaronic and bipolaronic bands, which facilitates the electrical conduction.

Although Bolto *et al.*[28] reported in 1963 polypyrrole derivatives with resistivity as low as 1 Ohm·cm, the discovery and development of conducting polymers were attributed to Shirakawa, MacDiarmid, Heeger, who reported the conductivity of polyacetylene doped with iodine,[29] when they awarded with the Novel Prize in Chemistry 2000. Generally, ECP are categorized in three groups: non-cyclic polyenes (*e.g.* polyacetylene), cyclic polyenes (*e.g.* poly(*p*-phenylene) and its derivatives), and polyheterocyclic ECP (e.g. polypyrrole (PPy), polythiophene (PTh), polyaniline (PAni)). The last group is actually considered the most versatile due to the excellent properties exhibited by such ECP, especially in terms of electrochemical and environmental stabilities. Figure 2 displays the chemical structure of the most representative ECP of each group.

Although chemical synthesis provides many different possible routes to obtain a variety of ECP, electrochemical synthesis is frequently the preferred alternative since this procedure is relatively straightforward and enables the control over the yielding, morphology and electrochemical properties of the resulting material. Some ECP, such as PPy and poly(3,4-ethylenedioxythiophene) (PEDOT), have been polymerized by both chemical and electrochemical processes, the advantages and disadvantages of both strategies being summarized in Table 1. Both procedures involve the oxidative polymerization of monomers dissolved in the medium by the action of a chemical oxidant or by applying an anodic potential at the electrode, respectively. The oxidative mechanism for polyheterocyclic ECP, as occurs in chemical and electrochemical polymerization processes, is summarized in Figure 3.

Because of the outstanding electrical, electrochemical, optical and magnetic properties shown by ECP,[24-26] these materials have been applied in a great number of technological fields that include organic optoelectronics,[30] organic photovoltaics,[31] energy storage technology,[32,332] and the fabrication of electrochromic[34] and electroluminescent[35] devices. Recently, as ECP have also extended to the biotechnological, bioengineering and biomedical fields,[36-39] special attention has been given to tailor desirable properties (*i.e.* electrical, chemical and physical properties) to better suit the nature of the specific bioapplication. For example, the ability to entrap and controllably release biological molecules through reversible doping, and the ability to transfer charge from a biochemical reaction are two of the promising inherent functions of ECP.

Currently, ECP are frequently used as biosensors, tissue-engineering scaffolds, neural probes, drug-delivery devices and bio-actuators, as it has been recently reviewed.[36-40] In particular, for tissue engineering applications, ECP show interesting

advantages but also some limitations (*i.e.* lack of mechanical integrity, absence of biodegradability and hydrophobicity).[37,40-42] ECP blending with conventional insulating polymers or biopolymers is the most popular approach followed to solve these drawbacks.[43-48] An alternative and also effective strategy, that was recently reviewed by Albersson and co-workers,[43] is the synthesis of new biodegradable polymers containing conducting oligomers. Due to the growing interest in this class of new biomaterials, the palette of degradable and electrically conductive polymers is progressively expanding to meet the demands of specific applications within the biomedical field. For example, in the last year Schmidt and co-workers reported biodegradable electroactive copolymers composed of oligoaniline-based blocks linked to polyethylene glycol or polycaprolactone blocks, which deliver anti-inflammatory drugs on the application of electrochemical stimuli.[49]

In this work we use the concepts discussed in the two previous sections to review the fabrication of FsNM for biomedical applications. Firstly, we will discuss the design and development of FsNM made of biopolymers and insulating polymers. After this, we will focus on FsNM fabricated by blending conventional polymers with ECP. Finally, several concluding remarks on the achievements and future perspectives of this outstanding research field will be exposed.

4. Biomedical Applications of Insulating and Electrochemically Inactive Free-Standing Nanomembranes

Generally, FsNM for biomedical applications are made using synthetic or naturally derived polymers. Among the synthetic ones, linear aliphatic polyesters, such as poly(lactic acid) (PLA) and poly(lactic-*co*-glycolic acid) (PLGA), have been extensively chosen since their biodegradation rate and mechanical properties can be easily controlled

through variations in their molecular weight.[50] Also, poly(ether ester) copolymers have been successfully employed due to their excellent properties (*e.g.* elasticity, toughness, strength and easy processability), which arise from the combination of both soft and hard segments along their chemical structure.[51] In regard to biopolymers, the most frequently used are collagen and polysaccharides, such alginate and chitosan, their applications being usually focused in tissue engineering.[52,53]

In the biomedical context, FsNM need from specific requirements such as biocompatibility and, in some cases, also biodegradability and/or bioresorbability need be met. Furthermore, by successfully controlling the chemical composition and the fabrication process, it is possible to tune and adjust the physicochemical, mechanical, chemical and morphological properties of FsNM to promote cell-substrate interaction, which is particularly relevant in regenerative medicine (*i.e.* cellular organization can be directly regulated through the cellular microenvironment).[54,55] Their structure and flexibility allows FsNM to coat the surface of devices that interact with biological systems or, alternatively, FsNM can be introduced in a needle by aspiration, and then be moved and released/injected in liquid environments (*e.g.* finely positioned on surgical incisions or directly used for wound treatments).

Next sub-sections review the most representative examples of FsNM made of insulating polymers for advanced biomedical applications. Table 2 summarizes their main characteristics, which are described below organized by polymeric families (namely, polyester, polysaccharide and other polymeric sources).

4.1. Polyester Free-Standing Nanomembranes

Takeoka and co-workers[56] developed PLA FsNM (Figure 4a) with a thickness of 23 ± 5 nm by spin-coating a PLA solution (5 mg/mL) at 4000 rpm for 20 s onto a poly(vinyl

alcohol) (PVA) sacrificial film. The mechanical properties and adhesion strength of the resulting transparent films, which exhibited a flat and uniform surface without cracks, were evaluated using the bulging test and microme-scratch test, respectively. These PLA-based FsNM showed low elastic modulus (1.7 ± 0.1 GPa) and high adhesiveness [the critical load for detachment of the nanosheet adsorbed onto a SiO_2 substrate was (1.7 ± 0.3)·10^5 N/m], which encouraged the analysis of their feasibility as a wound dressing in an *in vivo* experimental gastrostomy model test. Results were extremely positive, showing an excellent sealing efficacy that did not require adhesive agents. Moreover, the incision healed completely without scars and tissue adhesion. In an effort to deeply investigate the possible biomedical application of these PLA FsNM, their antiadhesive and fixative characteristics were further investigated: an intraperitoneal polypropylene overlaid mesh (IPOM) with PLA nanosheets was placed on an intact peritoneum (Figure 4b).[57] Results evidenced that PLA FsNM are feasible to induce adhesion prophylaxis in IPOM, having a beneficial effect as an atraumatic fixation tool. In addition, it was found that nanosheets do not cause inflammatory reaction, which was attributed to the excellent biocompatibility of PLA.[57]

Within this research line, in another study, Takeoka and co-workers[58] tested the feasibility of PLA FsNM as a wound dressing against burn infections in an *in vivo* mouse model partial-thickness injury. PLA FsNM tightly adhered onto the burn lesion on the mouse back without any adhesive agents, while adhesion to any opposing tissues/organs was not observed. Moreover, its transparency enabled the visual observation of the wound condition, and thus the infection evolution and healing process were easily monitored. In addition, PLA FsNM functioned as a barrier against *Pseudomonas. aeruginosa* when it was inoculated on the wound lesion. Therapy with PLA nanosheet

protected against an inflammatory response.[59] Hence, the tested system rendered an effective dressing material for the management of partial-thickness burn wounds.

More recently, the same group obtained PLA nanosheets by combining a spin-coating-assisted multi-layering process of PVA and PLA with a peeling step. Therefore, after the spin-coating and by dissolution of the sacrificial PVA layers between PLA layers in distilled water, a number of PLA FsNM which corresponded to the number of multi-layering processes of PVA and PLA were obtained.[59] The thickness of the resulting FsNM, which were transparent and extremely flexible, was determined to be 60 ± 6 nm when spin-coating a PLA solution (10 mg/mL) at 4000 rpm for 20 s. Later, these nanosheets were fragmented to form a stable suspension, and then reconstructed to form a single continuous film that attached to various interfaces without the need of adhesive agents (Figure 5). The new patched film was applied as a physical barrier against burn wound infection with *P. aeruginosa*. Both *in vitro* and *in vivo* assays evidenced that the patched film exhibited excellent barrier ability to prevent infection during the treatment of burns for 3 days.

With the aim of designing a novel patch for bone or tendon repair and healing, Pensabene *et al.*[60] studied the biocompatibility, adhesion and proliferation activity of several cell types onto PLA FsNM prepared by spin-coating (2 wt.% PLA solution in dichloromethane at 4000 rpm for 20 s using PVA as sacrificial layer). Their average thickness, which was assessed by AFM, was 320 ± 27 nm, while the elastic modulus, derived from bulge test experiments, was 136 ± 44 MPa. Both immortalized cell lines and primary cell lines cultured on those FsNM exhibited good morphological and metabolic features and the ability to fully differentiate. In addition to the *in vitro* assays, the adhesion of such PLA FsNM to ligament and femur was evidenced under *ex vivo* conditions using a rabbit model. Moreover, their short- and medium-term

biocompatibility was evaluated using C2C12 cultured cells.[61] Results evidenced early differentiation with the fusion of cells into firmly adherent myotubes, proving that such flexible nanofilms behaved as good bioactive matrices for cell anchoring, spreading and proliferation.

The effect of an underlying substrate on the interaction between cells and PLA FsNM was recently investigated.[62] For this purpose, polyester-based nanosheets (with thickness values from 29 ± 1 nm to 703 ± 4.4 nm, depending on the PLA concentration during the spin-coating process) were also fabricated by spin-coating and PVA acted as the sacrificial layer. After PLA FsNM releasing in a liquid environment, they were collected on stainless steel mesh (PLA-mesh), and subsequently used for cell adhesion studies using rat cardiomyocytes cells (H9c2). Results were compared to the ones obtained on a control interface: SiO_2 substrates coated with an ultra-thin layer of PLA (PLA-substrate). Although topological and mechanical properties of PLA FsNM did not influence the cell viability after 24h of culture, cells did geometrically sense the stiffness of the underlying material, thus affecting the adhesion geometry. Briefly, PLA-mesh induced an anisotropic adhesion of H9c2 cells along the metal wire, while H9c2 cells on PLA-substrate adhered isotropically, independently of the nanosheet thickness. Accordingly, cells distinguished the increase in the nanosheet stiffness and preferentially adhered onto the rigid interface. Interestingly, cellular anisotropy decreased by increasing the thickness of the PLA FsNM deposited onto the mesh because the nanosheet stiffness was more homogeneous throughout the surface. Considering the huge difference between the Young's modulus of PLA FsNM (from 3.5 ± 1.3 to 7-10 GPa depending on the thickness) and the metal substrate (hundreds of GPa), it was concluded that cell adhesion was mechanically regulated by the stiffness of the underlying substrate when the thickness of the PLA FsNM was in the order of tens of nanometers.

PLA FsNM have also been modified and/or functionalized by means of collagen deposition, magnetic particles entrapment and drug loading. In a recent study, Niwa *et al.*[63] prepared PLA nanosheets modifying only one surface with collagen to endow different discrete functions to each side of the nanosheet: anti-adhesive and pro-healing properties. For this purpose, PLA FsNM were prepared by spin-coating using conditions similar to those previously described (thickness: 59.5 ± 9.5 nm). A collagen layer was subsequently deposited on the surface following two approaches: solvent casting or spin-coating. The latter strategy resulted in an ultra-thin collagen coating (thickness of 5-10 nm) more homogeneous and hydrophilic than that obtained by solvent casting, which exhibited a thickness of ~120 nm. The disorganized collagen fibrils formed on PLA nanosheets when covered using the spin-coated method induced a hydrophilic microenvironment that improved cell adhesion and spreading, in comparison to that obtained by solvent casting. Besides, fine networks of actin filaments were clearly identified in cells cultured on the former biointerface, as opposed to the latter system.

As a first step to develop magnetic FsNM to be remotely controlled and manipulated, Taccola *et al.*[64] embedded superparamagnetic iron oxide nanoparticles (SPION) into PLA nanosheets by spin-coating (5-20 mg/mL PLA solution in chloroform and 1-15 mg/mL SPION colloidal solution at 3000 rpm for 20 s using a PVA sacrificial layer). Magnetic composites were coloured with different degrees of intensity depending on the nanoparticles load, and the inclusion of SPION in the polymeric matrix did not alter their magnetic behaviour, yielding FsNM with high saturation magnetization and magnetic susceptibility. For nanosheets with high concentration of SPION, the magnetic response increased because of the formation of clusters, albeit their presence did not alter the integrity and stability of the FsNM. Results were good enough to promote further

investigation in this area, suggesting that controllable supports with magnetic properties could be fabricated in a near future for biomedical applications.

FsNM with unidirectional drug delivery ability have the potential to improve therapeutic efficacy, while minimizing undesirable side effects. In this sense, Sun and co-workers[65] fabricated robust and flexible FsNM by sandwiching drug-containing polyelectrolyte multilayer films between a capping and a barrier layer of PLGA. The drug-containing films were prepared by the LbL assembly of chemically cross-linked poly(allylamine hydrochloride)−dextran (PAH-D) microgel and hyaluronic acid (HA), which can load methotrexate (MTX), a negatively charged cancer-inhibiting drug. The PLGA barrier layer, which was obtained by spin-coating, prevents MTX release, and the PLGA capping layer regulates the unidirectional MTX release kinetics in a precisely controlled manner. *In vitro* cancer treatments evidenced that MTX released from the FsNM preferentially inhibited the proliferation of HeLa cells. The versatility of LbL assembled polymeric films as drug carriers allows the loading of a wide variety of drugs and bioactive agents. Thus, the design of highly efficient unidirectional drug-delivery systems with minimizing side effects to normal tissues has a great potential for clinical applications.

Finally, Okamura *et al.*[66] prepared disk-shaped PLGA nanosheets and modified their surfaces with the dodecapeptide H12 (HLGGAKQAGDV), which is a fibrinogen γ-chain carboxy-terminal sequence (γ400-411) that specifically recognizes the active form of glycoprotein IIb/IIIa on activated platelets. Under flow conditions, H12-PLGA FsNM were found to interact with activated platelets on a collagen surface faster than H12-PLGA microparticles did. In addition, only FsNM induced 2D spreading of platelet thrombi on collagen-immobilized plates. These results suggested that PGLA FsNM might

be a suitable candidate as novel platelet substitutes and, also, an alternative to human platelet concentrates infused to treat bleeding in patients with severe thrombocytopenia.[66]

4.2. Polysaccharide Free-Standing Nanomembranes

Polysaccharides are a class of biological macromolecules that participate in a wide range of biochemical and biomechanical functions. Because of their unique properties, these biopolymers are currently playing an important role in materials science. The structure and function of polysaccharides, and their nanoscale assembly for biomedical materials were recently reviewed by Boddohi and Kipper. [67] However, this section will draw the attention to those studies that used polysaccharide as the main polymeric source to develop and design FsNM. As in the previous section, biomedical applications and promising results will be highlighted.

In 2007, Fujie, Okamura and Takeoka[68] constructed what they called a "nano-adhesive plaster", a multilayered FsNM (thickness: 30.2 ± 4.3 nm) made of chitosan and sodium alginate (Na-alginate) that was deposited onto a PVA-silicone rubber substrate using the spin-coating assisted LbL approach. More specifically, the layers of each polyelectrolyte were spin-coated on the silicone rubber (millimetre scale thickness: 1.0 mm) previously covered with a sacrificial PVA layer (microscale thickness: 1.2 μm). As a result, the nano-adhesive plaster consisted on the superposition of three different types of free-standing sheets (Figure 6a). Chitosan and Na-alginate contain amino and carboxylic groups, respectively, as cationic and anionic polyelectrolytes at ambient pH, which enormously facilitated their assembly in the FsNM. The elastic modulus, which was determined by the bulge test, was found to be 1.3 GPa. The good adhesiveness and flexibility of the nano-adhesive plaster was evidenced by transferring it, after modification with a luminescent pigment for ease of visibility, not only onto the skin of a

human arm[68] (Figures 6b-6d) but also onto a tissue (rat cecum) surface.[69] In a subsequent study, the same group proved the potential biomedical application of these this adhesive, robust and flexible nano-adhesive plasters made of chitosan and Na-alginate in a surgical intervention.[70] Thus, a FsNM with a thickness of 75 nm repaired an *in vivo* visceral pleura defect induced on beagle dogs without any loss in the respiratory function and without significant inflammatory response. In addition, the influence of the thickness in the mechanical properties of polysaccharide FsNM was demonstrated, which enabled an easy modulation of the nanosheet features.

Besides, the therapeutic effect of the nano-adhesive plaster on murine cecal puncture was evaluated (Figure 7).[71] The sealing effect of the multilayered chitosan and Na-alginate-based FsNM inhibited effectively the bacterial infection, and increased the survival rate of the individuals. Interestingly, the treatment with the polysaccharide nanosheet provoked less inflammatory response than the suture.[71] Despite the promising results, a small percentage of bacteria were able to pass thorough the FsNM. To overcome this aspect, an antibiotic-loaded polysaccharide nanosheet was developed.[72] In this new approach, an antibiotic (tetracycline, abbreviated TC) was sandwiched between a new PVA layer (named PVAc in Figure 8), which acted as a protector, and the LbL assembled polysaccharide platform (total thickness: 177 nm). The resulting FsNM, which comprehended three functional layers (Figure 8), exhibited an important anti-microbial effect and a relatively low inflammatory tissue response.[72] As a consequence, *in vivo* studies using overlapping therapy with these new PVA / TC / polysaccharide FsNM showed a significantly increase in mouse survival after cecal puncture. Later research evidenced that TC-loaded chitosan and Na-alginate multilayered FsNM exhibited a potential antibacterial activity when covering mice dorsal skin artificially burnt and infected with *P. aeruginosa*.[73] All mice treated with the TC-loaded polysaccharide FsNM

survived, whereas mice treated with TC-unloaded nanosheets and mice left untreated displayed increased rates of mortality due to bacterial infection. Moreover, TC-loaded FsNM prevented not only local inflammation but also systematic inflammation.

Hagisawa *et al.*[74] described a novel therapy in which the overlapping of several chitosan / Na-alginate FsNM with a thickness of 75 nm (*i.e.* multioverlapping therapy) sealed and stopped a massive venous hemorrhage on rabbits. Before *in vivo* tests, the mechanical durability of the nanosheets and its hydrostatic pressure resistance was evaluated. Four pieces of overlapping nanosheets were able to stand 80 ± 6 mm Hg of pressure. In regard to its degradability, polysaccharide nanosheets experience a decrease in their thickness in degradation conditions (phosphate-buffered saline, PBS, at 37 ºC). Nevertheless, they retained more than 70% of the thickness after seven days. Positively, after one month, no inflammatory tissue reaction was detected around the FsNM attachment and findings revealed a complete wound healing. The multioverlapping therapy would represent a great advantage for surgical operation, especially in trauma patients with bleeding from large veins.

Otani *et al.*[75] have reported the therapeutic use of bilayered polysaccharide FsNM made of chitosan and Na alginate as arachnoid plaster in a microneurosurgery environment because its semi-absorbent and potent physical adhesive strength features. These authors observed that the application of overlapping FsNM without using chemical bonding agents completely avoided cerebrospinal fluid leakages in the cerebral cortex. There was evidence of a relation between the number of overlaid nanosheets and the reinforcement effect: the more layers displayed, the more it improved. Besides, after six months, no inflammatory infiltration was detected.

In addition to chitosan and Na-alginate, proteoglycan HA has also been used to fabricate polysaccharide FsNM. For instance, Fujie *et al.*[76] prepared multilayered

nanosheets of HA and collagen on a water-soluble sacrificial supporting substrate using the LbL assembly method. The thickness of these FsNM was found to grow exponentially with the number of HA and collagen layers. This was attributed to the fact that the amount of HA adsorbed in the LbL structure is less than that of collagen.[77] Therefore, the polyion pairs mediated by the electrostatic interaction between collagen and HA molecules induced a nonlinear growth in the LbL system. The mechanical properties of these FsNM, as determined by the bulge test, were found to depend on the fibrous or non-fibrous structure of collagen layers. Thus, the elastic modulus of nanosheets made with non-fibrous collagen and a high content of HA (thickness: 62 ± 7 nm) was 4.3 ± 0.6 GPa, which is a value comparably smaller than that of the previously reported chitosan / Na-alginate nanosheet (9.6 GPa for a thickness of 75 nm[70]). This low elastic modulus was attributed to the hydrophilic and moisture-sensitive nature of HA molecules. In contrast, the elastic modulus of FsNM made with fibrous collagen (thickness: 42 ± 4), which had a low content of HA, increased to 12.5 ± 1.5 GPa, thus evidencing a greater mechanical durability. Collagen structures in bone and skin have an elastic modulus of 17.2 and 4 GPa, respectively. Therefore, FsNM made of HA and fibrous or non-fibrous collagen efficiently imitate the mechanical properties of these tissues. Consistently, FsNM made with non-fibrous collagen exhibited a surface with softer elastic properties than those observed in FsNM with fibrous collagen. Besides, cell adhesion studies using NIH-3T3 cells showed that HA / non-fibrous collagen FsNM gave lower cell adhesive elongation in comparison to nanosheets with fibrous collagen and a low content of HA. On the basis of this study, authors concluded that cell adhesive properties can be tuned by changing the structural components of the nanosheets (*i.e.* the content of polysaccharide and collagen fibrils),[76] thus opening a new door to the

production of novel engineered scaffolds for regenerative medicine as well as cell biology.

An innovative and audacious strategy has been recently reported by Chen *et al.*[78] who prepared cell-polymeric nanocomposites for the fabrication of FsNM lined with cells (Figure 9). First, poly(N-isopropylacrylamide) (PNIPAM), which is a temperature-responsive polymer, was grafted onto glass-slides. After this, cells were cultured on the resulting hydrophobic layer. Once 80-90% cell confluence was achieved, the LbL process was conducted on the surface of the cell sheet. However, gelatin, which is a natural biocompatible polyelectrolyte, was previously deposited as cell-contacting layer to keep a high cell viability during the deposition process.[79,80] Thus, this gelatin layer is of great importance during the LbL self-assembly step on the cell-sheet surface.[79,80] Specifically, three alternating charged polysaccharide bilayers of chitosan and Na-alginate, (chitosan/Na-alginate)$_3$, were assembled onto the gelatin-coated cells cultured on the PNIPAM-grafted surfaces. The deposition of gelatin, chitosan and Na-alginate layers, which are extra cellular matrix (ECM) related components, on the cell sheet resulted in a cell adhesive surface that efficiently interacted with cells.[81] The free standing cell/gelatin/(chitosan/Na-alginate)$_3$ film was peeled off from the PNIPAM-grafted surface upon temperature changes. By this strategy, the assembly of cell sheets with ultra-thin ECM components to form FsNM can be potentially used to fabricate complex artificial soft tissues to substitute some elements in native tissues.

4.3. Other Polymeric Sources for Free-Standing Nanomembranes

Poly(ethylene oxide) (PEO) is a thermoplastic biocompatible material widely used in biomedical applications, as for example scaffolds, drug delivery systems and sensor devices.[82-84] To extend their list applications, the LbL technique was used to fabricate

FsNM made of PEO.[85] This was achieved by creating solid-state hydrogen bonded assemblies that allowed the incorporation of stable interdigitated layers of PEO and poly(acrylic acid) (PAA) at the nanometer length scale (the thickness of each PEO/PAA bilayer was 80 nm). Free-standing films containing 100 bilayers were transparent, smooth to the touch and exhibited elastomeric properties during handling. Although these were not explicitly proved with experiments, Lutkenthaus *et al.*[85] suggested many biomedical applications for these hydrogen bonded assemblies, as for example biosubstrates, drug delivery devices and pH-sensitive sensors.

Ono and Decher[86] reported the use of pH-responsive self-standing polyelectrolyte multilayer membranes, which were fabricated by spraying polymer solutions, for biomedical applications. Concretely, a silicon wafer substrate was covered by a sacrificial multilayered film made of PAA and poly(ethylene glycol) (PEG), which disintegrated by a pH change releasing a target membrane. In that work, the released membrane consisted of a simple polyelectrolyte multilayered film of poly(allylaminehydrochloride) (PAH) and poly(sodium-4-styrenesulfonate) (PSS), which was initially constructed on the top of the PAA/PEG pH-responsive film. The pH response mechanism is based on the alteration of the hydrogen bonds established between PAA and PEG when the carboxylic acid groups present in PAA transform into carboxylate ions. From a biomedical point of view, the advantages of the PAA/PEG pH-responsive film, which were obtained with thickness values ranging from 55 to several hundreds of nanometers and areas of a few square centimetres, rely on the fact that PAA and PEG are biocompatible, biotolerated or bioinert. Accordingly, their release would not lead to adverse effects in the bioenvironment, and thus could be used in therapeutic devices and aids.

In another example, the preparation of PEG-terminal FsNM was based on the extensively cross-linking of aromatic 4'-nitro-1,1'-biphenol-4-thiol (NBPT) self-

assembled monolayers (SAM) deposited onto a gold support by exposure to low energy electrons, thus resulting in a mechanical and thermally stable monolayer.[87] Simultaneously, the terminal nitro groups of the NBPT molecules were converted to reactive amine moieties to which epoxy functionalized PEG chains were subsequently coupled. As a result, these films exhibited protein repelling properties, which in turn ensure the lack of protein denaturing when they are used as support in transmission electron microscopy studies.[87]

Meyerbröker and Zharnikov developed highly elastic, hydrophilic and ultra-thin membranes consisting entirely of PEG.[88] This was achieved by preparing an ultra-thin stable PEG-hydrogel precursor film composed of a mixture of epoxy- and amine-terminated PEG moieties, which was deposited onto a supported sacrificial layer (*i.e.* a 100 nm gold film evaporated onto a silicon substrate). Then, the complementary terminal groups underwent chemical crosslinking.[89] Afterwards, the PEG/gold bilayer was separated from the silicon support and the sacrificial layer was dissolved releasing the PEG FsNM, which could be transferred onto a grid or any other arbitrary substrate. These nanosheets exhibited sufficient mechanical stability, and also high flexibility (extraordinary low Young's modulus of only ~2 MPa). Such behavior is characteristic of elastomers,[90] and it was never observed before in nanomembranes. Indeed, the only analogous systems are polyisoprenes and polyisobutenes nanomembranes, which are not biocompatible, prepared using Langmuir-Blogett technology.[17] On the basis of their properties, PEG nanosheets are potentially useful as a highly sensitive support and sensor element for biological samples.

In another work, porous multilayered films of PAH and PAA were prepared using the LbL dipping technique, nanopores being subsequently created with a pH treatment.[11] The porosity induced by pH adjustment resulted in a significant increase in the thickness.

For example, the thickness of films made of 8 PAH/PAA bilayers before and after the creation of nanopores was 101 to and 253 nm, respectively. Ketoprofen and cytochalasin D, which represent different types of drugs that can be entrapped in these films, were successfully loaded and showed zero order release kinetics over a long period of time. The amount of drug loaded and released could be tuned by varying the number of bilayers in the porous regions of the films, whereas variations of the pore size controlled the release flux of a given drug. . On the other hand, sheet- and tube-like FsNM of PAA/PAH were prepared by exfoliating PAA/PAH multilayered films from substrates in an aqueous acid solution containing Cu^{2+}.[91] Initially, multilayered films were prepared by LbL deposition onto silicon wafer, quartz or glass tubes substrates. Their ion-triggered exfoliation was achieved by breaking the electrostatic interactions between the PAA layer and the underlying substrate. However, it should be noted that, although PAA/PAH bilayers were nanometric, ion-triggered exfoliation was applied to films with 15 bilayers of submicrometric thickness (~0.8 μm) and, therefore, these cannot be considered as nanomembranes. The developed technology was proposed for the fabrication of small-caliber artificial blood vessels.

Gui *et al.*[82] fabricated LbL multilayer films made of poly(diallyldimethylammonium) (PDDA) and poly(4-vinylpyridine propylsulfobetaine) (P4VPPS), a zwitterionic polysulfobetaine, in an acid aqueous solution at pH 2 with 0.5 M NaCl. The average growth rate was estimated to be ~29.0 nm per PDDA/P4VPPS bilayer. These films were pH-dependent, thus disintegrating in alkali aqueous solution, especially at pH ≥ 12, which suggested a potential application as sacrificial layers for the release of other polymeric films. This was proved by depositing a multilayered film of PDDA and poly(sodium 4-styrenesulfonate) (PSS) on the top of a 10-bilayered PDDA/P4VPPS sacrificial film. After treatment with alkali aqueous solution at pH 12, the PDDA/PSS film was released

keeping its integrity in air. Previously, Dubas *et al.*[93] had reported the fabrication of PDDA/PSS FsNM using PDDA/PAA LbL multilayer films as sacrificial layers.

Kohri *et al.*[94] presented a new approach for the fabrication of smooth and stable FsNM composed of a polymer brush, poly(2-hydroxyethyl methacrylate) (PHEMA), supported on a ultra-thin (*i.e.* ~6 nm) colourless polydopamine (PDA) layer. This was achieved through the surface-initiated atom radical polymerization (ATRP) of 2-hydroxyethyl methacrylate (HEMA) on the PDA layer, which resulted in optically transparent and colourless free-standing PHEMA brush films with tailored thickness of 16-75 nm. Previous to this process, the PDA ultra-thin film was placed onto a silicon or glass substrate covered by a cellulose acetate sacrificial layer (thickness: ~115 nm). The scheme of the synthetic design is displayed in Figure 10. Although no application was explicitly tested, authors suggested that PHEMA FsNM can be used as multi-stimuli responsive sensors after functionalizing their surface.[94]

Surface-functionalized FsNM were produced grafting poly(2-methacryloyloxyethyl phosphorylcholine) (PMPC) brushes by the ATRP of 2-methacryloyloxyethyl phosphorylcholine (MPC) on nanosheets made of PAH, PAA and PS, which were prepared by the spin-coating assisted LbL technique (thickness of 85 ± 2 nm).[95] The properties of PMPC-nanosheets (physiological stability, surface wettability and anti-biofouling response) were regulated by several parameters, such as the thermal crosslinking of the FsNM, the grafted amount of MPC and the thickness of PMPC brushes (*ca.* 11 nm). PMCP-nanosheets were easily peeled, transferred using tweezers with the aid of a water-soluble PVA sacrificial layer, cut into any shape by scissors, and patterned with a needle. Nanosheets patched on cell culture substrates exhibited anti-biofouling properties such as anti-coagulant behaviour of human blood cells as well as the potential to microscopically pattern murine fibroblasts cells. The overall of the results

provided an important physicochemical insight into the remarkable biological response of surface-functionalized nanosheets, which represent not only a powerful tool for biomedical applications but also an alternative to conventional micropatterned techniques used in bionanotechnology.

Fujie *et al.*[96] developed spatio-selective cell culture environments by inkjet printing bio-patterns onto FsNM composed of poly(methyl methacrylate) (PMMA). The thickness of the nanosheets, which were prepared by spin-coating, was *ca.* 200 nm. Interestingly, several cell adhesion promoters, such as poly(L-lysine) modified with fluoresceine isothiocyanate , were micropatterned on the FsNM surface and, subsequently, functionalized with fibronectin by electrostatic interaction. The high flexibility of PMMA FsNM provided an ideal substrate for cell adhesion and spreading. *In vitro* assays showed the selective deposition of C2C12 skeletal muscle myoblasts following these patterns. Accordingly, the protein micropatterned FsNM system was proposed as an interesting tool for cell-directed culture in muscular tissue engineering.

PMMA was also employed for the preparation of FsNM displaying phase separation morphology. This was achieved by spin-coating a polymer mixture solution of PMMA and polystyrene (PS) onto a PVA-coated substrate.[97] Due to the intrinsic immiscibility of PMMA and PS, rapid quenching during the spin-coating process induced their phase separation. In order to obtain porous nanosheets, PS regions were dissolved by immersing the PMMA-PS FsNM into cyclohexane. The thickness of these films, which ranged from 38.8 ± 1.1 to 110.2 ± 2.0 nm, and the diameter of the pore, which varied between 64.4 ± 9.3 and 187.2 ± 33.9 nm, were controlled through the PMMA:PS ratio and the spin-coating conditions. Furthermore, authors demonstrated that when the thickness of the ultra-thin films is comparable to the dimensional scale of the phase separation domains, it is possible to prepare perforated FsNM with nanopores in the range of tens of

nanometers.[97] The availability of these perforated FsNM is proposed to be of immense value in many biomedical applications, as for example cell culture devices, high flux biosensors and drug delivery systems.

Flexible PS FsNM for directing cellular organization were prepared by Fujie *et al.*[98] by combining spin-coating and microcontact printing methodologies. The PS nanosheet thickness, which ranged from tens to hundreds of nanometers, was controlled through the concentration of the polymer solution used during the spin-coating process. In this work, the sacrificial layer was made of PNIPAM. After hydrophilization of the PS nanosheet surface, a composite made of multi-walled carbon nanotubes and fibronectin (CNT-Fn) was micropartterned on the FsNM using poly(dimethyl siloxane) (PDMS) molds with microscopic groove-ridge features (width and separation of ~50 μm). Then, unpatterned regions were rendered cytophobic by Pluronic F-127 to promote initial cell alignment. As a result, the CNT-Fn nanocomposite was homogeneously distributed onto the flexible PS nanomembrane (Figure 11a). Nanomechanical mapping revealed the high flexibility of these engineered nanomembranes by simply decreasing the film thickness. This flexibility is illustrated in Figures 11b and 11c, which displays the bending of a silicone tube wrapped with a 40 nm thick PS/CNT-Fn FsNM. Therefore, the combination of their outstanding features (*i.e.* high flexibility, cell adhesiveness and surfaces with tailored morphology) suggests that such systems recreate the properties of the extracellular matrix (ECM). Cell-adhesive micropatterns facilitated the alignment of C2C12 skeletal myoblasts, while CNTs enhanced the cellular elongation and differentiation to generate functional myofibers.

In an earlier study, Tsukruk and co-workers[4,99] prepared hybrid organic-inorganic FsNM with extraordinary sensitivity and unique auto-recovering ability. These nanosheets (thickness of 25-70 nm) were prepared by spin-assisted LbL assembly of

PAH and PSS on a sacrificial substrate. The most innovative aspect of these FsNM is the intercalation of a central layer containing gold nanoparticles (diameter of 12.7 nm) sandwiched between PAH/PSS bilayers. Thus, the general formula of these nanosheets can be described as: $(PAH/PSS)_n$PAH-Au-$(PAH/PSS)_n$-PAH, were *n* was varied between 3 and 11. The thickness of the system with a gold central layer was ~20 nm higher than that of films without gold nanoparticles, independently of *n*. The mechanical properties of these hybrid FsNM (elastic modulus of 30-40 GPa, ultimate strain of about 2% and ultimate tensile strength higher than 100 MPa) were found to surpass those reported for a much thicker (*i.e.* submicrometer scale) nanoparticle-containing free-standing LbL films.[99] Moreover, the overall of the examined properties suggested a wide variety of prospective applications,[4] those related with the development of chemical and temperature micro-array sensors being particularly relevant in the biomedical field.

Metallic nanoparticles were also used to fabricate a superhydrophobic/hydrophilic asymmetric FsNM using the LbL approach on a Teflon substrate.[100] In this case, the layer assembly was achieved between a poly(ethyleneimine)-Ag^+ complex (PEI-Ag) at pH 9 and PAA at pH 3.2. The incorporated silver ions were reduced to silver nanoparticles during the thermal treatment applied to promote the cross-linking by imide bonds formation. As a result, silver loaded films displayed asymmetric wettability: the top surface was superhydrophobic, while the bottom one was hydrophilic. On the one hand, the superhydrophobic side limited the bacterial adhesion and exhibited self-cleaning properties; on the other, the hydrophilic side delivered bactericidal silver ions. These silver-functionalized hybrid films can be of great potential in open wound patches or in the barrier, separation, transportation or drug delivery field, although exceeding the nanoscale (thickness ranging between 2 and 20 μm, depending on the number of layers). That aspect was overcome by Hammond and coworkers,[101] who designed contact-killing

ionically cross-linked LbL ultra-thin films using N,N-dodecyl,methyl-polyethylenimine (DMLPEI), which has microbicide activity, layered with PAA (thickness < 100 nm for films with a number of bilayers ranging from 2 to 20). A pH treatment was applied during the assembly process to rearrange the microbicide polycation chains. Thus, at acid pH, the amount of positive charges on the surface available to interact with the bacterial cell membrane is higher than at neutral pH. Consistently, films as thin as 10 nm made at pH 3 were more lethal to both airborne and waterborne bacteria than films made at pH 7.

Baxamusa *et al.*[102] proposed the fabrication of FsNM without using any sacrificial layer for their release from the substrate. More specifically, these authors proposed the direct delamination of ultra-thin films made of poly(vinyl formal) (PVF) resin, PS or PMMA. Delamination of a thin film from its substrate spontaneously occurs when the strain energy (G_v) in the film exceeds the interfacial energy resisting separation (γ). In practice, this occurs when the film thickness (L) satisfies the following condition:[103]

$$L > 2\frac{1+\upsilon_f \gamma}{1-\upsilon_f E\varepsilon^2} \qquad (1)$$

where υ_f is the Poisson's ratio of the film, γ is the difference in interfacial energy between the laminated and delaminated state, E is the Young's modulus of the film, and ε is the strain mismatch between the film and the substrate. Delamination and capture on wire supports of extraordinarily thin and large polymeric thin films have been enhanced by decreasing the interfacial energy between the film and its deposition substrate through electrostatic adsorption of a cationic polyelectrolyte. By this procedure and using polydiallyldimethylammonium chloride (PDAC) as polyelectrolyte, the minimum delaminated film thickness for PVF, PS and PMMA was found to be 8, 12 and 15 nm, respectively. The characteristics of this methodology, which can be extrapolated to many

types of polymers, make the fabrication of FsNM for biomedical applications a potential scalable process.

Lastly, extraordinarily thin FsNM (thickness < 5 nm) were obtained by spatially confined polymerization of a unique and elaborate 2D supramolecular system composed of two liquid-crystalline lamellar bilayer membranes made of self-assembled nonionic surfactant, dodecylglyceryl itaconate (DGI), which was sandwiched by a water layer (Figure 12).[104] Nanosheets are achieved using a simple free-radical polymerization under UV radiation with high yield and in large quantity. The covalently bonded two-molecular-thick sheets exhibited a high mechanical strength and thermal stability. Moreover, an important characteristic of these ultra-thin sheets is the high-density of functional groups exposed to the outer surfaces. Post-functionalization of the hydroxyl groups at the head of DGI located on the outer surfaces of these nanomembranes, opens the door to many practical applications in the biomedical field.

5. Biomedical Applications of Free-Standing Nanomembranes with Electroactive Conducting Polymers

Human body tissues, such as neural, cardiac or skeletal muscle ones, respond to electrical and electrochemical stimuli, signals being able to regulate cell growth and behaviour. However, conventional biomaterials do not result in appropriate biointerfaces to conduct electrical and/or electrochemical stimulation since they lack of both electrical conductivity and electrochemical activity. In order to overcome this drawback, ECPs have been used as biocompatible materials which can support cell adhesion, migration and proliferation.[105] Their properties are of great potential since they can be used to electrically stimulate local tissue,[106-109] exchange ions reversibly with cells, thus promoting adhesion and proliferations of these living systems,[41,110,111] fabricate electronic

devices (*e.g.* biocapacitors and biobatteries) that can be implanted in the organism,[112] act as time controlled drug- or bactericidal-release devices,[113,114] detect biomolecules,[115-117] recognize specific fragments of DNA,[118,119] etc. Recently, Llorens *et al.*[120] reviewed the advances on the preparation of structures (*i.e.* essentially fibrous mats) based on biodegradable and ECPs for biomedical applications. On the other hand, it should be remarked that the electrochemical detection of biomolecules using ECP has received intense interest within the biomedical field.[121-126] In this application, ECP act as interfaces between bio-substrates and inorganic electrodes favouring lowered impedance between the electrode and electrolyte interface. Accordingly, as ECP-based biosensors consist of organic films (or even hydrogels) supported on inorganic electrodes rather than in self-supported organic membranes and, therefore, their discussion has not included in this review.

Nevertheless, one of the major drawbacks to obtain free-standing nanosheets composed exclusively of ECPs is the lack of mechanical integrity, poor stability, brittleness and the restricted processability of many of these materials. These limitations, combined with their non-degradability, affect the number of biomedical applications of all-ECP FsNM. Because of this reason, in this section we separate the few studies on FsNM fabricated only with ECPs and inorganic-ECP hybrids, from those based on insulating polymer-ECP blends.

The biomedical applications of some ECPs are limited by the biocompatibility and cytotoxicity of these materials, which in turn depend on their chemical nature. In a recent study, Humpolicek *et al.*[127] examined the biocompatibility of non-conducting and conducting PAni form (*i.e.* PAni emeraldine base and PAni hydrochloride, respectively). Although both forms of PAni did not induce any sensitization and skin irritation, the two materials but specially the PAni hydrochloride exhibited considerable cytotoxicity.

Polymer purification via re-protonation ↔ de-protonation cycles led to a significant reduction in cytotoxicity, suggesting that the negative effects were provoked by low molecular weight reaction residues or by oligomers rather than by the own PAni molecules. Subcutaneous implantation of PAni emeraldine base films into animal models showed inflammation response and fibrous encapsulation.[128,129] In opposition, PPy exhibited good biocompatibility. Wang *et al.*[130] evaluated the biocompatibility of PPy supported membranes with nerve tissue. PPy showed no evidence of acute and subacute toxicity, pyretogen, hemolysis, allergen and mutagenesis, and the cells showed better survival and proliferation rates than with the control saline solution. These results suggested that PPy might be a candidate material for bridging the peripheral nerve gap.[130] George *et al.*[131] evaluated the cytotoxicity of PPy *in vitro* using primary cerebral cortical cells and *in vivo* surgically implanting PPy substrates in the cerebral cortex of rats. Results evidenced that PPy is at least as biocompatible as Teflon (used as a control) and, in fact, performed better in many cases. Similarly, PTh and its derivatives have shown tremendous potential for interfacing electrically conducting polymers with biological applications due to their low cytotoxicity and high biocompatibility. For example, PEDOT[41] and poly(α-terthiophene)[132] (PTh_3) have been used to fabricate bioactive platforms, even though their monomers and small oligomers are cytotoxic. Cytotoxicity is particularly low for some water-soluble PTh derivatives bearing hydrophilic pendant moieties, which have been proposed as excellent lysosome-specific materials for bio-imaging applications.[133]

Despite its current importance among conducting materials and its recently developed biomedical applications, in this review we have not included studies based on graphene nanosheets.[134,135] Graphene typically presents porous and honeycomb-like structures and, in some cases, it has been considered as an alternative to ECPs in the

preparation of single component FsNM. However, the use of graphene is restricted by the topology of its bidimensional nanosheets, which is not comparable to that of ECP.[136,137]

5.1. All-Electroactive Conducting Polymers and Inorganic-Electroactive Conducting Polymer Free-Standing Nanomembranes

In spite of the fact that the mechanical properties of ECPs are in general poor, different strategies have been developed to produce free-standing membranes of micrometric thickness made of PPy,[138-142] PAni[143-145] and PTh[146-148] for their application in different fields, such as separation membranes, electrode materials, sensors and catalysts.

In 2010, Wang *et al.*[149] reported a novel one–pot procedure to prepare PPy FsNM which was based on an interfacial polymerization (IP) that occurred at the interface between air and a Cu^{2+}-containing ionic liquid (Figure 13a). Resulting films were compact and uniform, and exhibited finely controlled thickness, with values from tens to hundreds of nanometers (*i.e.* as low as 60 nm, Figure 13b). However, FsNM with a thickness under 50 nm were brittle and weak, and broke easily. PPy FsNM doped with *p*-toluenesulfonic acid (TSA) displayed good electrical properties. Specifically, the electrical conductivity of films with a thickness of ~230 nm was 1.14 S/cm, although this value was lower than that reported previously for PPy in other systems. Moreover, asymmetrical films with different smoothness and water wettability on each side of the film were also prepared by altering the concentration of Cu^{2+} ions in the liquid phase (Figure 13c). Even though no biomedical application was proposed by the authors, it is highly promising for this field the development of a general methodology for the preparation of ECP films with different hydrophilicity and roughness on each side.

Jeon *et al.*[150] fabricated PPy FsNM by organic crystal surface-induced polymerization of the monomer in an aqueous suspension containing hydrated crystals of sodium decylsulfonate below the Krafft temperature (*i.e.* temperature above which thermodynamic stable micelles are formed), and using $FeCl_3$ as oxidant (Figure 14a). The main role of the crystals was to act as a template onto which the polymerization occurred. FsNM obtained using this procedure were composed of a unique ECP domain with a thickness of ~21 nm, widths of 2-6 μm, and lengths greater than 10 μm (Figures 14b and 14c). The electrical conductivity of these nanosheets was determined to be 30.6 S/cm, thus one order of magnitude higher than the value displayed by spherical PPy nanoparticles (diameters 30-50 nm) prepared by emulsion polymerization (2.9 S/cm). Besides, the feasibility of PPy FsNM to perform as HCl and NH_3 vapour detectors was evaluated: the system exhibited high sensitivity and a fast response with respect to PPy nanoparticles, which was attributed to the increased surface area and porosity of the former nanostructure. Despite the fact that the application studied for PPy FsNM was not biologically related, the methodology used is of relevant importance to successfully obtain FsNM.

More recently, Qi *et al.*[151] developed PPy FsNM by *in situ* freezing interfacial polymerization (FIP). This approach differs from the conventional interfacial polymerization in that the chemical reaction takes place at a solid/liquid interface. In this specific work, water and cyclohexane, which are immiscible, were used as the liquid and solid phase, respectively; solid cyclohexane being achieved upon crystallization. Special attention was paid to the following issues: (1) the reaction temperature, which should be under lower than the freezing point of the organic solvent and water, but above that of the monomer; and (2) the minimization of the polymerization of the monomer and the formation of PPy particles before the formation of solvent crystals. FsNM were very

smooth and their thickness was about 100 nm. In this case, the electrical conductivity was determined to be 430 S/cm, whereas for the optimal synthetic conditions and doping parameters, the electrical conductivity reached peaks as high as 2010 S/cm, opening the door to potential biomedical applications such as biosensors.

Jha *et al.*[152] reported a novel strategy for the one-pot fabrication of PPy FsNM by dropping a dichloromethane solution that contained the monomer and a porphyrin derivative to an aqueous $FeCl_3$ solution kept in a beaker. Initially, a porphyrin/PPy bilayer formed spontaneously at the air/$FeCl_3$ interface, which after being washed rendered the PPy nanosheet. Following this method the nanosheet thickness can be tailored by changing the monomer concentration in the dropping solution. Hence, the thickness of the PPy FsNM prepared by Jha *et al.*[152] increased from 50 to 250 nm when the pyrrole concentration augmented from 0.01 to 1 M. In addition, the conductivity of these PPy FsNM, which initially was of only ~10^{-5} S/cm, was enhanced after optimizing the doping parameters (*i.e.* the conductivity improved by ~ 30 and ~150 times on exposure to hydrochloric acid and iodine, respectively). Most importantly, the conductivity of these nanosheets showed no change when kept in air for more than 6 months, revealing a very noticeable stability in air. Although no specific application was examined, potential applications were mentioned (*e.g.* biosensors and artificial muscles).

On the other hand, the number of studies devoted to PAni-based nanosheets, which mainly consist of PAni/inorganic hybrid composites, is very scarce and their application in the biomedical field is practically inexistent. For example, very recently, it was reported the fabrication of layered PAni/graphene/PAni nanosheets (the thickness of PAni and graphene layers was of 3.7 and 8.9 nm, respectively), which exhibited excellent gravimetric capacitance.[153] This sandwiched structure was essentially oriented towards applications in energy storage devices, solar cells, semiconducting devices, *etc.* Niu *et*

al.[154] used a "*skeleton/skin*" strategy for the preparation of free-standing, thin and flexible single-walled carbon nanotube (SWCNT)/PAni hybrid films by a simple *in situ* electrochemical polymerization method. In this approach, directly grown SWCNT films with a continuous reticulate structure acted as the template, whereas PAni layers acted as the skin. The resulting hybrid films displayed a much higher conductivity compared to that of SWCNT/PAni composite films based on the post-deposition of the SWCNT film. Flexible, thin and lightweight supercapacitors were fabricated using SWCNT/PAni hybrid films. Although the applications of PAni-based nanomembranes[153,154] were not related with biomedicine, the above described properties may be useful for the fabrication of energy storage components for biomedical equipment.

Regarding to PTh and its derivatives, Greco *et al.*[155] reported the preparation of FsNM made of PEDOT and PSS complexes (PEDOT/PSS), where PSS acted as the dopant agent. In this study, the Supporting Layer method, which enables the release and recovering of the free-standing nanosheet, was used (Figure 15). Firstly, a layer of water-soluble PVA is deposited as the sacrificial layer on a substrate (PDMS) by spin-coating. Then, the desired nanosheet is supported on that sacrificial layer. Later, once the bilayered film is dried, it is peeled off from the substrate. The thickness of those FsNM, which was controlled through the rotation speed, ranged from ~100 nm (rotation speed of 1000 rpm) to ~40 nm (rotation speed ≥ 4000 rpm). Moreover, the mechanical and electrical properties of PEDOT/PSS FsNM were extensively investigated as a function of their thickness. With decreasing thickness, the elastic modulus values, which were determined by the strain-induced buckling test, varied between 0.81 and 1.02 GPa, while the electrical conductivity decreased from 1.44 to 0.88 S/cm. Interestingly, solvent casted PEDOT/PSS micrometric films (thickness of 7.5 μm) showed a conductivity of 1.38 S/cm. Therefore, a percolation threshold was reached based on the microscopic grain-like

structure or the effect of residual water present in the FsNM. This is schematically illustrated in Figure 16, which shows that the interconnectivity between neighbour conductive particles is not improved in FsNM with increasing thickness. However, the stacking of multiple conductive grains in micrometric films results in an improved number of interconnections and long-range connectivity. Because of the proven biocompatibility of PEDOT,[41,156,157] PEDOT/PSS FsNM were considered as a first proof of concept towards the development of smart conductive substrates for cell growth and stimulation.[155] Although no cell culture study was reported in that work, PEDOT/PSS FsNM have been recently used to fabricate electrochemical microactuators in the form of microfingers of a variety of lengths.[158] The reversible actuation of these microactuators, which consists in the bending of such microfingers, has been demonstrated by imposing electrochemical oxidation and reduction cycles on PEDOT/PSS supports. A number of possible applications can be envisaged for these small, soft actuators, such as microrobotics for cell manipulation.

The same group embedded iron oxide superparamagnetic nanoparticles into PEDOT/PSS FsNM using the Supporting Layer method described above (Figure 15).[159] More specifically, a stable colloidal dispersion of iron oxide nanoparticles added to the PEDOT:PSS mixture was used to prepare nanofilms through spin-coating. The thickness and surface roughness of the nanosheets depended on the amount of incorporated nanoparticles, ranging from 218 ± 13 to 269 ± 19 nm and from 1.5 to 8.5 nm, respectively. In this investigation, the attention was focused on the characterization of the morphological, electrical, magnetic and magneto-optical properties, which also depended on the amount of entrapped iron oxide nanorparticles. The electrical conductivity was found to decrease from 1.96 ± 0.14 S/cm to 0.38 ± 0.06 S/cm with increasing concentration of nanoparticles. These FsNM open up new perspectives in technological

fields (electronics, telecommunications and optics) than can be successfully used for the construction of biomedical devices, even though no practical evidence for any application was provided.

PEDOT/PSS was also employed by Greco *et al.*[160] to prepare and characterize robust wrinkled conductive surfaces. This was achieved by following the simple two-step approach (metal deposition and subsequent heating) developed for the fabrication of nanowrinkles on shape-memory polymer sheets.[161] Specifically, the ECP nanosheet (thickness ranging from 53.6 ± 1.2 to 120.9 ± 1.5nm) was deposited onto a thermo-retractable PS sheet by spin-coating an aqueous dispersion of PEDOT:PSS. A subsequent thermal treatment induced the substrate shrinking causing the microbuckling of the upper PEDOT:PSS layer due to compressive stress patterning. Adhesion and proliferation assays of C2C12 murine skeletal cells on uniaxial wrinkled samples indicated that cells preferentially aligned on low and narrow ridges (~1.5 μm in height) rather than on high and wide ones (~2.5 μm in height). This observation was corroborated when aligned myotubes in C2C12 differentiation stage were only formed on the former topology. Furthermore, the co-culturing of C2C12 cells with a fibroblast feeder layer improved the formation of aligned and mature myotubes. The achievement of tuneable conductive nanowrinkled interfaces represents a unique tool for the development of innovative biomedical devices.

PEDOT has also been used to prepare mechanically robust, electrically conductive and transparent hybrid FsNM. This was achieved by Lee *et al.*,[162] who coated densified carbon nanotube sheets with PEDOT by vapour phase polymerization. For FsNM with a thickness of ~66 nm, the main properties were high mechanical strength and modulus (135 MPa and 12.6 GPa, respectively), low resistance (below 200 Ω per square), moderate optical transparency (56% at 550 nm wavelength), high flexibility and minor

changes in resistance upon bending. Another interesting characteristic of these FsNM was their remarkable shape-recovery ability in a liquid and at the liquid/air interface, as opposed to previous carbon nanotube sheets. On the basis of these properties, these hybrid PEDOT-containing FsNM were proposed to be of potential interest in the design of sensors, actuators, optical devices, fuel cells, as well as for electrochemical capacitors.

Ultra-thin films (thickness of 47 nm) of poly(3-thiophene methyl acetate) (P3TMA) have been prepared by spin-coating. For this system, the remarkable influence of the film-air interface in the thermal properties was examined by comparing the response of nanosheets and bulk P3TMA powder.[163] Although P3TMA, which is soluble in tetrahydrofuran, chloroform and dimethylformamide, among a few others, does not form free-standing films,[164] the understanding of its properties is of great interest because, as it will be discussed in the next sub-section, P3TMA has been combined with conventional biodegradable polymers to fabricate different types of electroactive FsNM with biomedical applications. Interestingly, the glass transition temperature determined using microcantilevers coated with ultra-thin P3TMA films resulted 5.2 ºC higher than that obtained for bulk powder samples. Moreover, ultra-thin films showed nanospherical aggregates of small (~40 nm) size, while powder bulk samples presented a micrometric granular morphology (Figure 17).

5.2. Insulating Polymer-Electroactive Conducting Polymer Free-Standing Nanomembranes

As mentioned above, blending of ECPs with insulating polymers is the most commonly followed approach to overcome the poor mechanical integrity of organic semiconductors. Accordingly, free-standing membranes have been fabricated by solvent casting mixtures of ECP with conventional insulating polymers, such as PVA[144] and

nylon 66.[165] However, in all cases, such membranes were of micrometric thickness and their potential use (*e.g.* optical pH sensors[144] and conductive coatings[165]) was not related to the biomedical field, even though they were prepared by combining ECP with biopolymers derived from natural sources. For example, cellulose-PAni membranes of micrometric thickness, which were prepared by *in situ* polymerization of aniline in the presence of bacterial cellulose nanofibrils, were used as electromagnetic interference shielding materials despite the biological origin of the biopolymer.[166] Table 3 summarizes the most relevant examples of ECP-containing FsNM, discussed in this section.

Armelin *et al.*[167] reported the preparation and characterization of FsNM that were obtained by spin-coating mixtures of a biodegradable polyester, poly(tetramethylene succinate) (PE44), and P3TMA. The thickness of these ultra-thin membranes, which ranged from 20 to 80 nm, was precisely controlled by adjusting the spin-coating process parameters and the solution concentration. It was proved that PE44-P3TMA FsNM retained both the biodegradability of PE44 and the semiconducting (~10^{-4} S/cm) and electrochemical properties of P3TMA. Calorimetric assays revealed that P3TMA and PE44 were only partially miscible, evidencing a phase separation. Thus, two glass transitions were identified in the mixture, even though they depended on the composition of PE44-P3TMA FsNM. Furthermore, the presence of P3TMA hindered the crystallization of PE44 and also affected the fusion of PE44 crystalline fraction. Nanosheets were found to be stable in air and ethanol for more than one year, which facilitates their manipulation. Preliminary cell culture results using epithelial cells (HEp-2) suggested that PE44-P3TMA FsNM are potential candidates for the fabrication of bioactive platforms with semiconducting response.

The good results obtained for PE44-P3TMA FsNM prepared using a 50:50 PE44:P3TMA molar ratio motivated further study on their potential application in the

biomedical field. More specifically, Pérez-Madrigal *et al.*[168] conducted an investigation devoted to quantify the following aspects related to these nanosheets: (1) their hydrolytic and enzymatic degradability; (2) their response towards different fibroblast and epithelial cellular lines; and (3) their electrochemical response when coated with cell monolayers. Hydrolytic and enzymatic degradation assays revealed the appearance of abundant crevasses and thin grooves after 4 weeks of immersion in phosphate buffered saline solution (PBS), these effects becoming more pronounced after 8 weeks (Figure 18a). Moreover, the weight loss of samples immersed in hydrolytic and enzymatic media indicates that the degradation rate is higher for the PE44-P3TMA blend than for the individual polyester (Figure 18b). This was attributed to the fact that in the blend the degradation of the polyester domains produced the detachment of P3TMA domains (labelled with white circles in Figure 18a. On the other hand, *in vitro* cellular adhesion and proliferation assays using HEp-2, MDCK, Cos-7 and Du-145 cell lines evidenced that PE44-P3TMA nanosheets behaved as potent cellular matrices (Figure 18c). Thus, the viability of cultured cells was higher, in terms of adhesion and proliferation, in blended FsNM than in individual PE44 and P3TMA ultra-thin films. Moreover, cyclic voltammetry studies reflected that PE44-P3TMA FsNM were electro-compatible with cellular monolayers, even though there was a slight reduction of the cathodic and anodic intensities. These features combined with the outstanding flexibility and robustness of the nanomembranes, which was demonstrated through aspiration in pipette/release/shape recovery cycles that were repeated without breaking the film (Figure 19), allowed the authors to propose the use of biodegradable PE44-P3TMA FsNM as bioactive platforms for tissue engineering.

Inspired by those promising results, Pérez-Madrigal *et al.*[169] replaced the polyester component in the preparation of PE44-P3TMA FsNM by an aromatic grade thermoplastic

polyurethane matrix (TPU). This was expected to improve the miscibility between the two components of the blend because of the presence of aromatic moieties in both polymers. Hence, TPU-P3TMA FsNM were prepared by spin-coating a TPU:P3TMA mixture with 40:60 weight ratio. The surface of the resulting nanosheets was described as the combination of the topographies of both individual components. This consisted in a homogeneous distribution of granules throughout the surface, which were associated with the P3TMA rich phase by conductive AFM (C-AFM) measurements (Figure 20). Moreover, TPU-P3TMA nanosheets showed well-localized folds homogeneously distributed, similarly to those also observed in individual TPU FsNM. As some films did not present folds, their formation was attributed to artefacts produced during the spin-coating process. The thickness of FsNM TPU-P3TMA ranged from 11 to 93 nm, while the average roughness was 16.3 ± 0.8 nm. Analysis of the mechanical properties indicated that the Young's modulus, which was determined by applying the Derjanguin–Müller–Toporov (DMT) contact mechanics, depended on the thickness of the nanomembranes. Thus, values determined for the thicker (80–140 nm) / thinner (10–40 nm) regions of TPU, P3TMA and blended ultra-thin films were 25 / 35 MPa, 3.5 / 12 GPa and 0.9 / 1.7 GPa, respectively. In contrast, the adhesion force was found to be homogeneous throughout the whole surface of TPU and P3TMA films (average values: 7.2 and 5.0 nN, respectively), while it depended on the phase distribution in case of TPU-P3TMA FsNM. The potential utility of these FsNM for tissue engineering applications was proved by cellular proliferation assays using Cos-7 cells. Results showed that TPU-P3TMA FsNM was more active as a cellular matrix than each of the two individual polymers.

In a subsequent study, the same authors[170] examined the electronic, electric and electrochemical response of the above mentioned TPU-P3TMA FsNM. Interestingly, the

optical band gap energy of these blended nanofilms was very similar to that obtained for individual P3TMA (*i.e.* E_g = 2.35 and 2.32 eV, respectively). This similarity, which did not occur when comparing the E_g value of the TPU:P3TMA mixture with that of P3TMA dissolved in THF, was attributed to the influence of the spin-coating process on the π-conjugation length and packing interactions of P3TMA chains (*i.e.* ECP chains are not able to adopt their equilibrium conformation because the solvent is completely evaporated). On the other hand, the electrical conductivity of TPU-P3TMA FsNM, determined by C-AFM measurements, was found to range from $2.23 \cdot 10^{-5}$ to $5.19 \cdot 10^{-6}$ S/cm. These inhomogeneous values were consistent with the presence of insulating TPU chains in P3TMA-rich domains. The voltammetric response of TPU-P3TMA FsNM and P3TMA was similar in terms of the ability to exchange charge reversibly and their electrochemical stability. On the basis of these results, authors proposed that TPU-P3TMA FsNM were excellent candidates to be used in tissue regeneration applications as biointerfaces to conduct electrical or electrochemical stimulation.[170]

Following this research line, in a very recent study,[171] special emphasis was given to determine the influence of TPU-P3TMA FsNM composition in those properties typically related to biomedical applications, such as swelling, resistance to hydrolytic and enzymatic degradation, and biocompatibility. Therefore, TPU-P3TMA FsNM samples with different TPU:P3TMA compositions (20:80, 40:60 and 60:40 weight ratios) were studied. Structural investigations based on morphological and topographical analyses evidenced that the 20:80 sample exhibited a surface similar to that obtained for individual P3TMA, while 40:60 and 60:40 FsNM presented an irregular distribution of prominent and well-localized folds like individual TPU. The water uptake of nanosheets decreased with the concentration of TPU, even though it was relatively high in all cases. Consistently, hydrolytic and enzymatic degradation increased with the P3TMA content

(Figures 21a and 21b). Moreover, TPU-P3TMA blends behaved as biodegradable materials. Viability assays evidenced that, although all TPU-P3TMA compositions provided biocompatible blends, the viability of cells increased with the concentration of TPU in the composition (Figures 21c and 21d). The overall of the results allowed the authors to conclude that 40:60 TPU-P3TMA FsNM was the most appropriated system for tissue engineering applications.

A completely different strategy to obtain FsNM made of an ECP and an insulating polymer is the one in which both components are arranged in a bilayered configuration. Greco *et al.*[172] fabricated self-supported nanosheets with patterned conductivity using PEDOT/PSS and PLA, which acted as the mechanical support layer, thus maintaining continuity and robustness. In a first step, the PEDOT/PSS layer (thickness of ~45 nm) was spin-coated onto a substrate. Then, in a second step, and after thermal treatment, the PLA layer (thickness of ~200 nm) was spin-coated onto the previous one. Nevertheless, n order to obtain a patterned bilayer FsNM, an intermediate step (inject patterning) was introduced just before the deposition of the PLA layer (*i.e.* localized over-oxidation of PEDOT/PSS nanofilm to provoke an irreversible loss of electrical conductivity at specific spots). Moreover, to enhance its electrical conductivity, which reached values of 180 S/cm, DMSO was added as a secondary doping agent. The resulting bilayered FsNM is of great interest as (bio)electrical interface and as thin floating or ultraconformable circuit. In addition to that, the surface wettability of the bilayered FsNM was electrochemically switched through simple oxidation and reduction processes. This change was even more evident for nanosheets supported on a PS substrate. On the basis of this interesting ability, authors proposed the application of these FsNM as smart conductive biointerfaces for directing cell adhesion and differentiation.[172]

A similar approach was followed by Pérez-Madrigal *et al.*[171] to prepare bilayered FsNM made of TPU-P3TMA and collagen. However, in this case, the role of the collagen layer was not to provide robustness, which was an intrinsic property of TPU-P3TMA FsNM, but to enhance the cellular response towards the TPU-P3TMA biointerface. Therefore, the TPU-P3TMA/collagen bilayer was formed by incubating a spin-coated TPU-P3TMA (40:60 weight ratio) layer in a collagen solution. . Amazingly, the adsorbed collaged layer was found to form two layers (Figure 22). The the top layer exhibited a pseudoregular honeycomb 2D network with cavities of different diameters (*i.e.* ranging from 194 ± 55 nm to 1.2 ± 0.7 μm) and depths *ca.* 73 nm, whereas, in contrast, collagen adopted a much more compact structure in the bottom layer. According to previous studies,[173,174] TPU-P3TMA/collagen biointerfaces were proposed as suitable scaffolds for biological and biomedical purposes. Similarly, a collagen layer was recently used to inhibit the cytotoxic effects of the remaining monomer leaking from a supported PTh_3 film, the resulting PTh_3/collagen biointerface behaving as bioactive platforms.[132]

5.3. A Challenge: Electroactive Conducting Polymers Free-Standing Nanomembranes for Energy-Based Biomedical Applications

In the 21st century, fuel cells have emerged as smart storage systems or alternatives energy conversion devices due to both their efficiency and the lack of pollutants emission in comparison with the coal combustion engines.[175] Currently, the development of new materials and fabrication processes to improve the effectivity of fuel cells and reduce their cost are important areas of research within this field. Application of ECP in fuel cell electrodes was proposed as a promising remedy to solve some of the problems identified in such energy store and generation systems, as for example chemical long-term stability

of the catalytic support and stable mechanical-structural stability.[176] Four different types of applications can be identified depending on the use of ECP in fuel cell electrodes:

- Support: ECP as obtained or structured (e.g. nanofibers and microspheres) act supporting the catalyst. For example, Pd-PAni nanofibers showed excellent electrocatalytic activity for the oxidation of methanol, ethanol and formic acid,[177] and Pt incorporated into poly(3-methylthiophene) showed effective dispersion of the catalyst and high catalytic activity in methanol oxidation.[178]
- Coating: the ECP coats a structured support of another material. For example, graphene nanosheets coated with PAni and decorated with Pt nanoparticles show high activity in the reduction of O_2 and oxidation of methanol, glucose and H_2O_2.[179]
- Part or a composite: For example simultaneous deposition of Pt and Ru on PEDOT doped with polystyrene-4-sulfonate yielded an active electrocatalyst for methanol oxidation.[180,181]

Some of these fuel cell applications of ECP are based on membranes separating the anodic (fuel) compartment from the cathodic (oxidant) compartment. However, the thickness of polymeric membranes in current fuel cells is in the micrometre scale[176,182] and, therefore, out of the scope of this review. In spite of this, recent advances in the FsNM field should be also considered as a strong driving force to look for alternative strategies for energy production. The biocompatibility, chemical and dimensional stability, and mechanical properties of FsNM discussed in previous sub-sections should motivate the scientific community to develop inexpensive and high-performing membranes for the fabrication of biological fuel cells. These devices could be considered from two points of view: (1) macroscopic devices with biological microorganisms

participating in the energy production; or (2) biological microorganisms with nanosheets, incorporated as electrode membranes, acting as micrometric biofuel cells. The latter may result in a new field based originated by the combination of energy and biomedicine.

Another promising field is the development of artificial muscles using ECP films. In this application, which is based on the transduction of electrical or electrochemical energy into mechanical work, electrochemical reactions in ECP films provoke dimensional variations that result in bending or linear macroscopic movements. The simple way to transduce reversible length variations in films of ECP into macroscopic movement is through a bilayer ECP/passive layer. The passive layer can be a tape,[183,184] a sputtered metal,[185,186] a piece of paper,[187] ECP/plastic,[188] or solid state electrolyte.[189] Electrochemically driven length variations in the film of ECP produce stress gradients across the two films interface and subsequently result in macroscopic bending, as is schematically illustrated in Figure 23. More specifically, for ECP exchanging anions with the electrolyte the film gives anticlockwise movement by oxidation (swelling) and clockwise during the reduction, while ECP exchanging cations produce clockwise movement by oxidation (shrinking) and anticlockwise by reduction of the ECP.[190] Artificial muscles based on ECP were recently reviewed by Otero and co-workers.[191] Unfortunately, at present time all biomimetic artificial muscles based on ECP have been prepared using free-standing membranes of micrometric thickness, as occurred for fuel cell electrodes. However, the increasing evolution in biomimetic reactive devices has resulted in the opening of new technological forefronts and challenges, including the application of FsNM.[191]

6. Conclusions and Perspectives

This review of FsNM for biomedical applications demonstrates the versatility of these simple nanostructures, in which molecules organize in a 2D configuration. Moreover, it highlights several ideas: (i) the variety of techniques available for their preparation, (ii) the concept that the rational design of nanostructured materials can be utilized to obtain tailored properties, and (iii) the relationship between the features of the nanosheets and their application. Although the list of biomedical applications for self-supported nanosheets is very extensive (*e.g.* wound dressing, patches for bone or tendon repair, scaffolds for regenerative medicine and tissue engineering, magnetically controllable bioactive platforms, drug delivery systems, platelet substitutes, devices for overlapping therapy, artificial soft tissues, biosensors, supports for biological samples, biointerfaces, coatings with microbicide properties, artificial muscles, microactuators for cell manipulation, bioelectrodes), investigation on such nanostructured organizations is still in its early stages, and many treasures still await scientific discovery.

Research in FsNM for biomedical applications, which began about one decade ago, has been essentially focused in using insulating polymers. From a practical point of view, studies have been conducted considering only two families of biodegradable materials: (1) polyesters, mainly PLA (*i.e.* PLGA and PE44 nanosheets were also sporadically chosen), and (2) polysaccharides. The inflammatory response provoked by FsNM made of these materials tends to be very low (*i.e.* lower than that of sutures), which of particular importance for therapeutic applications. Even though a few works with other materials have been reported (*e.g.* PEG, PAA, PDDA, P4VPPS and PMMA), these involve polymeric families with very different and disperse properties and, therefore, a general rationalization of the derived conclusions is not an easy task. Within this context, comparative studies to extract general conclusions are imperative. Biomedical applications of FsNM made of ECP have emerged with great interest in the last few years

(*i.e.* the first work appeared in 2010, even though most works are from 2013 onwards). Consequently, the number of ECP studied so far, individually or combined with insulating polymers, is still limited and much more effort is necessary in this direction.

In spite of the studies based on polysaccharides, the preparation of FsNM by combining synthetic polymers and biomolecules, such as proteins and DNA, is an unexplored field. Depending on the desired application, nanosheets with an heterogeneous or homogeneous distribution of the two components (*i.e.* polymer/biomolecule layers or polymer-biomolecule composites, respectively) may be designed. Not only could be the role played by the polymer in these FsNM to provide mechanical robustness but also to protect biomolecules against too fast biodegradation. Besides, if it was an ECP, it could also induce electrochemical, electrical or optical activity. However, the biological component would be the main protagonist and, therefore, responsible for the functionality and biomedical application of such nanosheets. For this purpose, both the number of possibilities and the palette of biocompounds offered by nature are immense. In addition, novel and effective advanced biomedical applications that reach the society cannot be obtained using synthetic polymers alone, thus significant studies related to the combination of synthetic and natural compounds are desirable, and should be a main research focus.

Regarding to ECP-containing nanostructured materials, biomedical applications centred in electrophysiology is a field that needs to be further explored. One of the central goals of electrophysiology is to offer tools that can monitor and manipulate bioelectrical activities in the human brain. In particular, implantable neural prostheses aim to replace or restore lost motor functions after disease or disability. Since the brain has soft curvilinear surfaces, properties of conductive FsNM discussed above are appropriate for the development of flexible bioelectronics interfaces. Hence, by a rational design, flexible

ECP-containing FsNM may be used to establish conformal contact in cerebral cortex. Another electrophysiological application of these flexible nanosheets is the integration of nanoelectronics in 3D polymer scaffolds for cell cultures. The merging of flexible nanoelectronics and cells would allow the monitoring of biological signals for clinical uses.

FsNM made with unique optical, electrical and magnetic properties can be fabricated using organic-inorganic composites, in which nanoparticles, nanowires, carbon nanotubes, clay platelets or other nanocolloids are combined with insulating or conducting polymers. Although a few studies have been reported in this field, developments are still in a very early stage. For example, organic-inorganic nanosheets could be interfaced with proteins and cells to produce complexes of nanostructured and biological entities with specific and finely tuned functions for a broad range of applications in diagnosis and treatment.

Finally, concerning the architecture of FsNM, it is necessary to explore the advantages provided by new techniques. For example, a procedure to obtain perforated nanosheets at the nanometric scale has been recently reported, as it was discussed above. However, the enormous potentiality of these FsNM remains completely unknown from a technological point of view. Moreover, much effort needs to be devoted to integrate new techniques for modifying or patterning the surface of nanosheets not only in already developed biomedical applications, but also in the development of new ones. For example, surface modification to functionalize and/or re-orient polymer molecules in ECP-containing nanosheets is expected to offer numerous opportunities as active biomedical interfaces.

In summary, numerous scientific and technical challenges for the design of FsNM abound, and it can be foreseen that their development for biomedical applications will continue to be a research area of growing interest.

7. Acknowledgements

Authors are in debt to supports from MINECO and FEDER (MAT2012-34498 and MAT2012-36205) and Generalitat de Catalunya (XRQTC). M.M.P.-M. thanks financial support through a FPI-UPC grant.

8. References

1. R. Langer, *J. Biomed. Mater. Res.*, 2013, **101A**, 2449.

2. S. Fleischer and T. Dvir, *Curr. Opin. Biotechnol.*, 2013, **24**, 664.

3. T. Cohen-Karni, R. Langer and D. S. Kohane, *ACS Nano*, 2012, **6**, 6541.

4. C. Jiang, S. Markutsya, Y. Pikus and V. V. Tsukruk, *Nat. Mater.*, 2004, **3**, 721.

5. J. D. Kittle, C. Wang, C. Qian, Y. Zhang, M. Zhang, M. Roman, J. R. Morris, R. B. Moore and A. R. Esker, *Biomacromolecules*, 2012, **13**, 714.

6. M. G. Bellino, I. Tropper, H. Duran, A. E. Regazzoni and G. J. A. A. Soler-Illia, *Small*, 2010, **6**, 1221.

7. J. A. Jaber, P. B. Chase and J. B. Schlenoff, *Nano Letters*, 2003, **3**, 1505.

8. C. S. Hajicharalambous, J. Lichter, W. T. Hix, M. Swierczewska, M. F. Rubner and P. Rajagopalan, *Biomaterials*, 2009, **30**, 4029.

9. Z. Tai, H. Ma, B. Liu, X. Yan and Q. Xue, *Colloids Surf., B*, 2012, **89**, 147.

10. S. Y. Wong, Q. Li, J. Veselinovic, B.-S. Kim, A. M. Klibanov and P. T. Hammond, *Biomaterials*, 2010, **31**, 4079.

11. M. C. Berg, L. Zhai, R. E. Cohen and M. F. Rubner, *Biomacromolecules*, 2006, **7**, 357.

12. K. C. Wood, J. Q. Boedicker, D. M. Lynn and P. T. Hammond, *Langmuir*, 2005, **21**, 1603.

13. H. Watanabe, E. Muto, T. Ohzono, A. Nakao and T. Kunitake, *J. Mater. Chem.*, 2009, **19**, 2425.

14. K. D. Sattler, Ed. *Handbook of Nanophysics.*, Vol. 5. Functional Nanomaterials., CRC Press. Taylor and Francis Group. , Boca Raton, FL 2011.

15. G. Decher, J. D. Hong and J. Schmitt, *Thin Solid Films*, 1992, **210–211**, 831.

16. G. Decher, *Science*, 1997, **277**, 1232.

17. G. Decher, Y. Lvov and J. Schmitt, *Thin Solid Films*, 1994, **244**, 772.

18. R. W. Corkery, *Langmuir*, 1997, **13**, 3591.

19. D. B. Hall, P. Underhill and J. M. Torkelson, *Polym. Eng. Sci.*, 1998, **38**, 2039.

20. I. Gurrappa and L. Binder, *Sci. Technol. Adv. Mater.*, 2008, **9**, 043001.

21. A. D. Stroock, R. S. Kane, M. Weck, S. J. Metallo and G. M. Whitesides, *Langmuir*, 2002, **19**, 2466.

22. W. Cheng, M. J. Campolongo and S. J. Tan, D. Luo, *Nano Today*, 2009, **4**, 482.

23. C. Jiang and V. V. Tsukruk, *Adv. Mater.*, 2006, **18**, 829.

24. T. A. Skotheim, R. L. Elsenbaumer, J. R. Reynolds, J. R. Handbook of conducting polymers, Marcel Dekker, New York, 1998.

25. C. Li, C. Bai and G. Shi, *Chem. Soc. Rev.*, 2009, **38**, 2397.

26. D. W. Hatchett and M. Josowicz, *Chem. Rev.*, 2008**, 108**, 746.

27. J. L. Bredas and G. B. Street, *Acc. Chem. Res.*, 1985, **18**, 309.

28. B.A. Bolto, R. McNeill and D.E. Weiss, *Aust. J. Chem.*, 1963, **16**, 1090.

29. H. Hirakawa, E. J. Louis, A. G. MacDiarmid, C. K. Chiang and A. J. Heeger, *J. Chem. Soc., Chem. Commun.*, 1977, 578.

30. Y. Xu, F. Zhang and X. Feng, *Small*, 2011, **7**, 1338.

31. B. Kippelen and J.-L. Brédas, *Energy Environ. Sci.*, 2009, **2**, 251.

32. Y. Xuan, M. Sandberg, M. Berggren and X. Crispin, *Org. Electron.*, 2012, **13**, 632.

33. D. Aradilla, F. Estrany, F. Casellas, J. I. Iribarren and C. Alemán, *Org. Electron.*, 2014, **15**, 40.

34. D. Aradilla, J. Casanovas, F. Estrany, J. I. Iribarren and C. Alemán, *Polym. Chem.*, 2012, **3**, 436.

35. H.-E. Yin, C.-H. Wu, K.-S. Kuo, W.-Y. Chiu, C.-F. Lee, N.-T. Li and P.-J. Chen, *Synth. Met.*, 2011, **161**, 1878.

36. N. K. Guimard, N. Gomez and C. E. Schmidt, *Prog. Polym. Sci.*, 2007, **32**, 876.

37. A.-D. Bendrea, L. Cianga and I. Cianga, *J. Biomater. Appl.*, 2011, **26**, 3.

38. R. Ravichandran, S. Sundarrajan, J. R. Venugopal, S. Mukherjee and S. Ramakrishna, *J. R. Soc. Interface*, 2010, **7**, S559.

39. J. Jaguar-Grodzinski, *e-Polymers*, 2012, **12**, 722.

40. C. Rincón and J. C. Meredith, *Macromol. Biosci.*, 2010, **10**, 258.

41. L. J. del Valle, F. Estrany, E. Armelin, R. Oliver and C. Alemán, *Macromol. Biosci.*, 2008, **8**, 1144.

42. L. J. del Valle, D. Aradilla, R. Oliver, F. Sepulcre, A. Gamez, E. Armelin, C. Alemán and F. Estrany, *Eur. Polym. J.*, 2007, **43**, 2342.

43. B. Guo, L. Glavas and A.-C. Albertsson, *Prog. Polym. Sci.*, 2013, **38**, 1263.

44. G. Shi, M. Rouabhia, Z. Wang, L. H. Dao and Z. Zhang, *Biomaterials*, 2004, **25**, 2477.

45. L. Huang, X. Zhuang, J. Hu, L. Lang, P. Zhang, Y. Wang, X. Chen, Y. Wei and X. Jing, *Biomacromolecules*, 2008, **9**, 850.

46. S. I. Jeong, I. D. Jun, M. J. Choi, Y. C. Nho, Y. M. Lee and H. Shin, *Macromol. Biosci.*, 2008, **8**, 627.

47. E. Llorens, M. M. Pérez-Madrigal, E. Armelin, L. J. del Valle, J. Puiggalí and C. Alemán, *RSC Adv.*, 2014, **4**, 15245.

48. M. Planellas, M. M. Pérez-Madrigal, L. J. del Valle, S. Kobauri, R. Katsarava, C. Alemán and J. Puiggalí, *Polym. Chem.*, 2015, **6**, 925.

49. J. H. Hardy, D. J. Mouser, N. Arroyo-Currás, S. Geissler, J. K. Chow, L. Nguy, J. M. Kim and C. E. Schmidt, *J. Mater. Chem. B*, 2014, **2**, 6809.

50. K. M. Nampoothiri, N. R. Nair and R. P. John, *Bioresource Technol.*, 2010, **101**, 8493.

51. K. Odelius, P. Plikk and A.-C. Albertsson, *Biomacromolecules*, 2005, **6**, 2718.

52. F. Khan and S. R. Ahmad, *Macromol. Biosci.*, 2013, **13**, 395.

53. R. Parenteau-Bareil, R. Gauvin and F. Berthod, *Materials*, 2010, **3**, 1863.

54. S. Martino, F. D'Angelo, I. Armentano, J. M. Kenny and A. Orlacchio, *Biotechnol. Adv.*, 2012, **30**, 338.

55. C. Zhao, A. Tan, G. Pastorin and H. K. Ho, *Biotechnol. Adv.*, 2013, **31**, 654.

56. Y. Okamura, K. Kabata, M. Kinoshita, D. Saitoh and S. Takeoka, *Adv. Mater.*, 2009, **21**, 4388.

57. K. Fujino, M. Kinoshita, A. Saitoh, H. Yano, K. Nishikawa, T. Fujie, K. Iwaya, Kakihara, S. Takeoka, D. Saitoh and Y. Tanaka, *Surg. Endosc.*, 2011, **25**, 3428.

58. H. Miyazaki, M. Kinoshita, A. Saito, T. Fujie, K. Kabata, E. Hara, S. Ono, S. Takeoka and D. Saitoh, *Wound Rep. Reg.*, 2012, **20**, 573.

59. Y. Okamura, K. Kabata, M. Kinoshita, H. Miyazaki, A. Saito, T. Fujie, S. Ohtsubo, D. Saitoh and S. Takeoka, *Adv. Mater.*, 2013, **25**, 545.

60. V. Pensabene, S. Taccola, L. Ricotti, G. Ciofani, A. Menciassi, F. Perut, M. Salerno, P. Dario and N. Baldini, *Acta Biomater.*, 2011, **7**, 2883.

61. L. Ricotti, S. Taccola, V. Pensabene, V. Mattoli, T. Fujie, S. Takeoka, A. Menciassi and P. Dario, *Biomed. Microdevices*, 2010, **12**, 809.

62. T. Fujie, L. Ricotti, A. Desii, A. Menciassi, P. Dario and V. Mattoli, *Langmuir*, 2011, **27**, 13173.

63. D. Niwa, T. Fujie, T. Lang, N. Goda and S. Takeoka, *J. Biomater. Appl.*, 2012, **27**, 131.

64. S. Taccola, A. Desii, V. Pensabene, T. Fujie, A. Saito, S. Takeoka, P. Dario, A. Menciassi and V. Mattoli, *Langmuir*, 2011, **27**, 5589.

65. D. Chen, J. Chen, M. Wu, H. Tian, X. Chen and J. Sun, *Langmuir*, 2013, **29**, 8328.

66. Y. Okamura, Y. Fukui, K. Kabata, H. Suzuki, M. Handa, Y. Ikeda and S. Takeoka, *Bioconjugate Chem.*, 2009, **20**, 1958.

67. S. Boddohi and M. J. Kipper, *Adv. Mater.*, 2010, **22**, 2998.

68. T. Fujie, Y. Okamura and S. Takeoka, *Adv. Mater.*, 2007, **19**, 3549.

69. S. Takeoka, Y. Okamura, T. Fujie and Y. Fukui, *Pure Appl. Chem.*, 2008, **80**, 2259.

70. T. Fujie, N. Matsutani, M. Kinoshita, Y. Okamura, A. Saito and S. Takeoka, *Adv. Funct. Mat.*, 2009, **19**, 2560.

71. T. Fujie, M. Kinoshita, S. Shono, A. Saito, Y. Okamura, D. Saitoh and S. Takeoka, *Surgery*, 2010, **148**, 48.

72. T. Fujie, A. Saito, M. Kinoshita, H. Miyazaki, S. Ohtsubo, D. Saitoh and S. Takeoka, *Biomaterials*, 2010, **31**, 6269.

73. A. Saito, H. Miyazaki, T. Fujie, S. Ohtsubo, M. Kinoshita, D. Saitoh and S. Takeoka, *Acta Biomater.*, 2012, **8**, 2932.

74. K. Hagisawa, A. Saito, M. Kinoshita, T. Fujie, N. Otani, S. Shono, Y.-K. Park and S. Takeoka, *J. Vasc. Surg. Venous Lymphat. Disord.*, 2013, **1**, 289.

75. N. Otani, M. Kinoshita, T. Fujie, A. Saito, S. Takeoka, D. Saitoh, K. Hagisawa, H. Nawashiro and K. Shima, *J. Clin. Neurosci.*, 2013, **20**, 301.

76. T. Fujie, S. Furutate, D. Niwa and S. Takeoka, *Soft Matter*, 2010, **6**, 4672.

77. C. Picart, J. Mutterer, L. Richert, Y. Luo, G. D. Prestwich, P. Schaaf, J.-C. Voegel and P. Lavalle, *Proc. Natl. Acad. Sci. U. S. A.*, 2002, **99**, 12531.

78. J. Chen, X. Qiu, L. Wang, W. Zhong, J. Kong and M. M. Q. Xing, *Adv. Funct. Mater.*, 2014, **24**, 2216.

79. P. T. Hammond, *Adv. Mater.*, 2004, **16**, 1271.

80. F. Caruso, R. A. Caruso and H. Möhwald, *Science*, 1998, **282**, 1111.

81. M. Matsusaki, K. Kadowaki, T. Nakahara and M. Akashi, *Angew. Chem. Int. Ed.*, 2007, **46**, 4689.

82. L. Ma, D. Li and J. Chen, *Drug Dev. Ind. Pharm.*, 2014, **40**, 845.

83. B. L. Seal, T. C. Otero and A. Panitch, *Mat. Sci. Eng. R*, 2001, **34**, 147.

84. L. Moroni, J. R. de Wijn and C. A. van Blitterswijk, *J. Biomater. Sci. Polym. Ed.*, 2008, **19**, 543.

85. J. L. Lutkenhaus, K. D. Hrabak, K. McEnnis and P. T. Hammond, *J. Am. Chem. Soc.*, 2005, **127,** 17228.

86. S. S. Ono and G. Decher, *Nano Lett.***,** 2006, **6**, 592.

87. N. Meyerbröker, Z.-A. Li, W. Eck and M. Zharnikov, *Chem. Mater.*, 2012, **24**, 2965.

88. N. Meyerbröker and M. Zharnikov, *Adv. Mater.*, 2014, **26**, 3328.

89. N. Meyerbröker, T. Kriesche and M. Zharnikov, *ACS Appl. Mater. Interfaces*, 2013, **5**, 2641.

90. F. Mallwitz and W. A. Goedel, *Angew. Chem. Int. Ed.*, 2001, **40**, 2645.

91. Y. Ma, J. Sun and J. Shen, *Chem. Mater.*, 2007**, 19**, 5058.

92. Z. Gui, J. Qian, B. Du, M. Yin and Q. An, *J. Colloid Interf. Sci.*, 2009, **340**, 35.

93. S. T. Dubas, T. R. Farhat and J. B. Schlenoff, *J. Am. Chem. Soc.*, 2001, **123**, 5368.

94. M. Kohri, Y. Shinoda, H. Kohma, Y. Nannichi, M. Yamauchi, S. Yagai, T. Kojima, T. Taniguchi and K. Kishikawa, *Macromol. Rapid Commun.*, 2013, **34**, 1220.

95. T. Fujie, H. Haniuda and S. Takeoka, *J. Mater. Chem.*, 2011, **21**, 9112.

96. T. Fujie, A. Desii, L. Ventrelli, B. Mazzolai and V. Mattoli, *Biomed. Microdevices*, 2012, **14**, 1069.

97. H. Zhang and S. Takeoka, *Macromolecules*, 2012, **45**, 4315.

98. T. Fujie, S. Ahadian, H. Liu, H. Chang, S. Ostrovidov, H. Wu, H. Bae, K. Nakajima, H. Kaji and A. Khademhosseini, *Nano Letters*, 2013, **13**, 3185.

99. C. Jiang, S. Markutsya and V. V. Tsukruk, *Adv. Mater.*, 2004, **16**, 157.

100. L. Shen, B. Wang, J. Wang, J. Fu, C. Picart and J. Ji, *ACS Appl. Mater. Interfaces*, 2012, **4**, 4476.

101. S. Y. Wong, Q. Li, J. Veselinovic, B.-S. Kim, A. M. Klibanov and P. T. Hammond, *Biomaterials*, 2010, **31**, 4079.

102. S. H. Baxamusa, M. Stadermann, C. Aracne-Ruddle, A. J. Nelson, M. Chea, S. Li, K. Youngblood and T. I. Suratwala, *Langmuir*, 2014, **30**, 5126.

103. L. B. Freund, S. Suresh, Thin Film Materials: Stress, Defect Formation and Surface Evolution; Cambridge University Press: Cambridge, UK, 2003.

104. H. Qin, D. Wang, X. Xiong and J. Jin, *Macromol. Rapid Commun.*, 2014, **35**, 1055.

105. P. R. Bidez, S. Li, A. G. MacDiarmid, E. C. Venancio, Y. Wei and P. I. Lelkes, *J. Biomater. Sci. Polym. Ed.*, 2006, **17**, 199.

106. I. Jun, S. Jeong and H. Shin, *Biomaterials*, 2009, **30**, 2038.

107. J. Huang, X. Hu, L. Lu, Z. Ye, Q. Zhang and Z. Luo, *J. Biomed. Mater. Res. A*, 2010, **93A**, 164.

108. J. Y. Lee, C. A. Bashur, C. A. Milroy, L. Forciniti, A. S. Goldstein and C. E. Schmidt, *IEEE Trans. Nanobiosci.*, 2012, **11**, 15.

109. C. R. Broda, J. Y. Lee, S. Sirivisoot, C. E. Schmidt and B. S. Harrison, *J. Biomed. Mater. Res. A*, 2011, **98A**, 509.

110. A.-D. Bendrea, G. Fabregat, J. Torras, S. Maione, L. Cianga, L. J. del Valle, I. Cianga and C. Alemán, *J. Mater. Chem. B*, 2013, **1**, 4135.

111. E. Llorens, M. M. Pérez-Madrigal, E. Armelin, L. J. del Valle, J. Puiggalí and C. Alemán, *RSC Adv.*, 2014, **4**, 15245.

112. D. E. López-Pérez, D. Aradilla, L J. del Valle and C. Alemán, *J. Phys. Chem. C*, 2013, **117**, 6607.

113. B. Teixeira-Dias, L. J. del Valle, D. Aradilla, F. Estrany and C. Alemán, *Macromol. Mater. Eng.*, 2012, **297**, 427.

114. G. Fabregat, B. Teixeira-Dias, L. J. del Valle, E. Armelin, F. Estrany and C. Alemán, *ACS Appl. Mater. Interfaces*, 2014, **6**, 11940.

115. G. Fabregat, E. Armelin and C. Alemán, *J. Phys. Chem. B*, 2014, **118**, 4669.

116. M. Martí, G. Fabregat, F. Estrany, E. Armelin and C. Alemán, *J. Mater. Chem.*, 2010, **20**, 10652.

117. G. Fabregat, E. Córdova-Mateo, E. Armelin, O. Bertran and C. Alemán, *J. Phys. Chem. C*, 2011, **115**, 14933.

118. S. Radhakrishnan, C. Sumathi, A. Umar, S. J. Kim, J. Wilson and V. Dharuman, *Biosens. Bioelectron.*, 2013, **47**, 133.

119. B. Teixeiras-Dias, D. Zanuy, J. Poater, M. Solà, F. Estrany, L. J. del Valle and C. Alemán, *Soft Matter*, 2011, **7**, 9922.

120. E. Llorens, E. Armelin, M. M. Pérez-Madrigal, L. J. del Valle and C. Alemán, *Polymers*, 2013, **5**, 1115.

121. X. F. Lu, W. J. Zhang, C. Wang, T.-C Wen and Y. Wei, *Prog. Polym. Sci.*, 2011, **36**, 671.

122. G. Fabregat, E. Córdova-Mateo, E. Armelin, O. Bertran and C. Alemán, *J. Phys. Chem. C*, 2011, **115**, 14933.

123. C. Z. Liao and F. Yan, *Polym. Rev.*, 2013, **3**, 352-406.

124. M. Marti, G. Fabregat, F. Estrany, C. Alemán and E. Armelin, *J. Mater. Chem.*, 2010, **20**, 10652.

125. L. Li, Y. Shi, L. J. Pan, Y. Shi and G. H. Yu, *J. Mater. Chem. B*, 2015, **3**, 2920.

126. L. Kergoat, B. Piro, D. T. Simon, M. C. Pham, V. Noel and M. Berggren, *Adv. Mater.*, 2014, **26**, 5658.

127. P. Humpolicek, V. Kasparkova, P. Saha and J. Stejskal, *Synth. Met.*, 2012, **162**, 722.

128. C.H. Wang, Y.Q. Dong, K. Sengothi, K.L. Tan, E.T. Kang, *Synth. Met.*, 1999, **102**, 1313.

129. M. Mattioli-Belmonte, G. Giavaresi, G. Biagini, L. Virgili, M. Giacomini, M. Fini, F. Giantomassi, D. Natali, P. Torricelli, R. Giardino, *Int. J. Artif. Organs*, 2003, **23**, 1077.

130. X. Wang, X. Gu, C. Yuan, S. Chen, P. Zhang, T. zhang, J. Yao, F. Chen and G. Chen, *J. Biomed. Mater. Res.*, 2004, **68A**, 411.

131. P. M. George, A. w. Lyckman, D. A. LaVan, A. Hedge, Y. Leung, R. Avasare, C. Testa, P. M. Alexander, R. Langer and M. Sur, *Biomaterials*, 2005, **26**, 3511.

132. S. Maione, G. Fabregat, L. J. del Valle, A.-D. Bendrea, L. Cianga, I. Cianga, I.; F. Estrany and C. Alemán, *J. Polym. Sci., Part B: Polym. Phys.*, 2015, **53**, 239.

133. F. Wang, M. Li, B. Wang, J. Zhang, Y. Cheng, L. Liu, F. Lv and S. Wang, *Sci. Rep.*, 2015, **5**, 7617.

134. S. Yin, Y. Goldovsky, M. Herzberg, L. Liu, H. Sun, Y. Zhang, F. Meng, X. Cao, D. D. Sun, H. Chen, A. Kushmaro and X. Chen, *Adv. Funct. Mater.*, 2013, **23**, 2971.

135. T. Nishikawa, R. Ookura, J. Nishida, K. Arai, J. Hayashi, N. Kurono, T. Sawadaishi, M. Hara and M. Shimomura, *Langmuir*, 2002, **18**, 5734.

136. Y. Zhang, T. R. Nayak, H. Hong and W. Cai, *Nanoscale*, 2012, **4**, 3833.

137. Y. Yang, A. M. Asiri, Z. Tang, D. Du and Y. Lin, *Mater. Today*, 2013, **16**, 365.

138. J. Lei, Z. Li, X. Lu, W. Wang, X. Bian, T. Zheng, Y. Xue and C. Wang, *J. Colloid Interface Sci.*, 2011, **364**, 555.

139. T. F. Otero and M. J. Ariza, *J. Phys. Chem. B*, 2003**, 107**, 13954.

140. D. Chowdhury, A. Paul and A. Chattopadhyay, *Langmuir*, 2005, **21**, 4123.

141. Y. Lu, G. Shi, C. Li and Y. Liang, *J. Appl. Polym. Sci*., 1998, **70**, 2169.

142. J. Song, H. Liu, M. Wan, Y. Zhu and L. Jiang, *J. Mater. Chem. A*, 2013, **1**, 1740.

143. B. Zhao, K. G. Neoh, F. T. Liu and E. T. Kang, *Langmuir*, 1999**, 15**, 8259.

144. I. Mihai, F. Addiego, D. Ruch and V. Ball, *Sensors Actuat. B-Chem.*, 2014, **192**, 769.

145. G.-W. Huang, H.-M. Xiao, H.-Q. Shi and S.-Y. Fu, *J. Polym. Sci. Part A: Polym. Chem.*, 2012, **50**, 2794.

146. R. Yue, S. Chen, B. Lu, C. Liu and J. Xu, *J. Solid State Electrochem.*, 2011, **15**, 539.

147. H. Zhu, L. Gao, M. Li, H. Yin and D. Wang, *Electrochem. Commun.*, 2011, **13**, 1479.

148. G. Shi, S. Jin, G. Xue and C. Li, *Science*, 1995, **267**, 994.

149. D. Wang, Y.-X. Li, Z. Shi, H.-L. Qin, L. Wang, X.-F. Pei and J. Jin, *Langmuir*, 2010, **26**, 14405.

150. S. S. Jeon, H. H. An, C. S. Yoon and S. S. Im, *Polymer*, 2011, **52**, 652.

151. G. Qi, L. Huang and H. Wang, *Chem. Commun.*, 2012, **48**, 8246.

152. P. Jha, S. P. Koiry, V. Saxena, P. Veerender, A. K. Chauhan, D. K. Aswal and S. K. Gupta, *Macromolecules*, 2011, **44**, 4583.

153. Z. Tong, Y. Yang, J. Wang, J. Zhao, B.-L. Su and Y. Li, *J. Mater. Chem. A*, 2014, **2**, 4642.

154. Z. Niu, P. Luan, Q. Shao, H. Dong, J. Li, J. Chen, D. Zhao, L. Cai, W. Zhou, X. Chen and S. Xie, *Energ. Environ. Sci.*, 2012, **5**, 8726.

155. F. Greco, A. Zucca, S. Taccola, A. Menciassi, T. Fujie, H. Haniuda, S. Takeoka, P. Dario and V. Mattoli, *Soft Matter*, 2011, **7**, 10642.

156. M. H. Bolin, K. Svennersten, X. Wang, I. S. Chronakis, A. Richter-Dahlfors, E. W. H. Jager and M. Berggren, *Sens. Actuators, B*, 2009, **142**, 451.

157. K. Svennersten, M. H. Bolin, E. W. H. Jager, M. Berggren and A. Richter-Dahlfors, *Biomaterials*, 2009, **30**, 6257.

158. S. Taccola, F. Greco, B. Mazzolai, V. Mattoli and E. W. H. Jager, *J. Micromech. Microeng.*, 2013, **23**, 117004.

159. S. Taccola, F. Greco, A. Zucca, C. Innocenti, C. de Julián Fernández, G. Campo, C. Sangregorio, B. Mazzolai and V. Mattoli, *ACS Appl. Mater. Interfaces*, 2013, **5**, 6324.

160. F. Greco, T. Fujie, L. Ricotti, S. Taccola, B. Mazzolai and V. Mattoli, *ACS Appl. Mater. Interfaces*, 2013, **5**, 573.

161. C. -C. Fu, A. Grimes, M. Long, C. G. L. Ferri, B. D. Rich, S. Ghosh, S. Ghosh, L. P. Lee, A. Gopinathan and M. Khine, *Adv. Mater.*, 2009, **21**, 4472.

162. J. A. Lee, M. K. Shin, S. H. Kim, S. J. Kim, G. M. Spinks, G. G. Wallace, R. Ovalle-Robles, M. D. Lima, M. E. Kozlov and R. H. Baughman, *ACS Nano*, 2012, **6**, 327.

163. O. Ahumada, M. M. Pérez-Madrigal, J. Ramirez, D. Curcó, C. Esteves. A. Salvador-Matar, G. Luongo, E. Armelin, J. Puiggalí and C. Alemán, *Rev. Sci. Instrum.*, 2013, **84**, 053904.

164. A. L. Gomes, J. Casanovas, O. Bertran, J. S. de C. Campos, E. Armelin and C. Alemán, *J. Polym. Res.*, 2011, **18**, 1509.

165. R. A. Khalkhali and M. B. Keivani, *Asian J. Chem.*, 2005, **17**, 835.

166. J. A. Marins, B. G. Soares, M. Fraga, D. Müller and G. M. O. Barra, *Cellulose*, 2014, **21**, 1409.

167. E. Armelin, A. L. Gomes, M. M. Pérez-Madrigal, J. Puiggalí, L. Franco, L. J. del Valle, A. Rodríguez-Galán, J. S. d. C. Campos, N. Ferrer-Anglada and C. Alemán, *J. Mater. Chem.*, 2012, **22**, 585.

168. M. M. Pérez-Madrigal, E. Armelin, L. J. del Valle, F. Estrany and C. Alemán, *Polym. Chem.*, 2012, **3**, 979.

169. M. M. Pérez-Madrigal, M. I. Giannotti, G. Oncins, L. Franco, E. Armelin, J. Puiggalí, F. Sanz, L. J. del Valle and C. Alemán, *Polym. Chem.*, 2013, **4**, 568.

170. M. M. Pérez-Madrigal, M. I. Giannotti, E.Armelin, F. Sanz and C. Alemán, *Polym. Chem.*, 2014, **5**, 1248.

171. M. M. Pérez-Madrigal, M. I. Giannotti, L. J. del Valle, L. Franco, E. Armelin, J. Puiggalí, F. Sanz and C. Alemán, *ACS Appl. Mater. Interfaces*, 2014, **6**, 9719.

172. F. Greco, A. Zucca, S. Taccola, B. Mazzolai and V. Mattoli, *ACS Appl. Mater. Interfaces*, 2013, **5**, 9461.

173. J. George, J. Onodera and T. Miyata, *J. Biomed. Mater. Res., Part A*, 2008, **87**, 1103.

174. J. George, Y. Kuboki and T. Miyata, *Biotechnol. Bioeng.*, 2006, **95**, 404.

175. D. J. Kim, M. J. Jo and S. Y. Nam, *J. Ind. Eng. Chem.*, 2015, **21**, 36.

176. R. Holze and Y. P. Wu, *Electrochim. Acta*, 2014, **122**, 93.

177. R. K. Pandey and V. Lakshminarayanan, *J. Phys. Chem. C*, 2009, **113**, 21596.

178. B. Rajesh, K. R. Thampi, J. M. Bonard, A. J. McEvoy, N. Xanthopoulus, H. J. Mathieu and B. Viswanathan, *J. Power Sources*, 2004, **133**, 155.

179. J.-D Qiu, L. Shi, R. P. Liang, G.-C. Wang and X. H. Xia. *Chem. Eur. J.*, 2012, **18**, 7950.

180. C. Arbizzani, M. Biso, E. Manferrari and M. Mastragostino, *J. Power Sources*, 2008, **180**, 41.

181. C. Arbizzani, M. Biso, E. Manferrari and M. Mastragostino, *J. Power Sources*, 2008, **178**, 584.

182. A. Kraytsbergs and Y. Ein-Eli, *Energy Fuels*, 2014, **28**, 7303.

183. T. F. Otero, E. Angulo, J. Rodriguez and C. Santamaria, *J. Electroanal. Chem.*, 1992, **341**, 369.

184. Q. B. Pei and O. Inganäs, *Adv. Mater.*, 1992, **4**, 277.

185. E. W. H. Jager, E. Smela and O. Inganäs, *Science*, 2000, **290**, 1540.

186 E. W. H. Jager, O. Inganäs and I. Lundstrom, *Science*, 2000, **288**, 2335.

187. S. D. Deshpande, J. Kim and S. R. Yun, *Smart Mater. Struct.*, 2005, **14**, 876.

188. S. J. Higgins, K. V. Lovell, R. M. G. Rajapakse and N. M. Walsby, *J. Mater. Chem.*, 2003, **13**, 2485.

189. G. Alici, A. Punning and H.R. Shea, *Actuat. B-Chem.*, 2011, **157**, 72.

190. L. Valero Conzuelo, J. Arias-Pardilla, J. V. Cauigh-Rodríguez, M.A. Smit and T. F. Otero, *Sensors*, 2010, **10**, 2638.

191. T. F. Otero, J. G. Martínez and J- Arias-Pardilla, *Electrochim. Acta*, 2012, **84**, 112-128.

CAPTIONS TO FIGURES

Figure 1. Schematic illustration of the (a) LbL and (b) spin-coating processes.

Figure 2. General classification of ECP and chemical structure of the more representative compounds of each group.

Figure 3. Mechanism for heterocyclic ECP polymerization, A= N–H and S for PPy and PTh, respectively.

Figure 4. (a) PLA FsNM with a thickness of 23 ± 5 nm prepared by Takeoka and co-workers:[56] macroscopic image of the nanosheet suspended in water (left) and SEM image of the nanosheet on an anodisc membrane (right). Reproduced with permission.[56] Copyright 2009, Wiley-VCH. (b) Technique of overlaying a PLA FsNM on a large-pore polypropylene mesh for intraperitoneal onlay mesh (IPOM) without a fixation suture: (1) Mesh placed on the peritoneum of a rabbit; (2) Overlaying of a PLA FsNM supported by a water soluble PVA sacrificial layer on which the letter "P" is written to distinguish the PLA side; (3) Dissolution of the PVA substrate with saline (arrow); and (4) After dissolution of the PVA film, the letter "P" is not visible. Reproduced with permission.[57] Copyright 2011, Springer.

Figure 5. Patched PLA FsNM coming from several fragmented nanosheets: (a) Macroscopic (i) and microscopic (ii, iii) images of fragmented PLA nanosheets adhered on a SiO_2 substrate using a digital camera, a digital microscope, and a scanning electron microscope, respectively; (b) Detachment of fragmented PLA FsNM from a poly(tetrafluoroethylene) plate. Reproduced with permission.[59] Copyright 2013, Wiley-VCH.

Figure 6. (a) Elements used to fabricate the nano-adhesive plaster floating in acetone: silicone rubber (substrate), PVA sheet (sacrifial layer) and polyssacharide FsNM photographed in the dark (polysaccharide FsNM was modified with luminiscent pigment

for ease visibility). Nano-adhesive plaster on the human skin (b) before the polysaccharide FsNM was released from the silicone rubber and (c) after release from such substrate. (d) Same image as (d) except that it was captured in the dark. Reproduced with permission.[68] Copyright 2007, Wiley-VCH.

Figure 7. FsNM made of chytosan and Na-alginate were applied to a murine model of cecal puncture: (a) cecal defect site punctures with a needle (dashed line circle showing an actual puncture site); (b) sealing with the polysaccharide nanosheet supported by a sacrifial PVA film, in which the letter "P" was written; (c) dissolution of the PVA film with saline water solution; and (d) after dissolution of the sacrificial layer, the letter "P" is not visible. Reproduced with permission.[71] Copyright 2010, Elsevier.

Figure 8. Preparative scheme for tetracycline (TC) loaded polysaccharide nanosheets made of chitosan and Na-alginate.

Figure 9. Schematic illustration of fabrication of cell/gelatin/(chitosan/Na-alginate)$_3$ FsNM.

Figure 10. Schematic representation of the preparation of a free-standing polymer brush film based on a colorless PDA thin layer: (a) spin-coating of sacrificial cellulose acetate layer onto silicon plate; (b) creation of colorless PDA thin layer containing an ATRP-initiating group; (c) construction of polymer brushes on the substrate by surface initiating ATRP; (d) recovery of polymer brush film based on a PDA layer by the dissolution of the cellulose acetate layer in DMF; and (e) photographic image of the obtained free-standing PHEMA brush film floating in dimethylformamide. Reproduced with permission.[94] Copyright 2013, Wiley-VCH.

Figure 11. (a) Schematic of preparation of PS nanomembranes with micropatterned CNT-Fn nanocomposites and aligned C2C12 myoblasts. Macroscopic and magnified fluorescent images of the nanomembranes (40 nm thick) wrapping a silicone tube (3 μm

diameter) (b) before and (c) after bending the tube. The micropatterns (rhodamine labeled fibronectin) were flexible and adhered to the curvature of the tube in the bending state. Reproduced with permission.[98] Copyright 2013, American Chemical Society.

Figure 12. Schematic illustration for the formation of free-standing, single-bilayer-thick polymeric nanosheets derived from DGI: (a) freeze-fracture electron microscopy image of DGI system, and, (b) top-view schematic showing cross-linking between DGI along one lamellar plane. Reproduced with permission.[104] Copyright 2014, Wiley-VCH.

Figure 13. (a) Schematic illustration of the formation of a film at the air/ionic liquid interface. (b) High magnification of the cross-sectional SEM images of the PPy FsNM. Top-view SEM image of (c) the rough side and (d) the smooth side of the film. (Inset) Water contact angle, showing values of 115º and 80º for the rough and smooth sides, respectively. Reproduced with permission.[149] Copyright 2010, American Chemical Society.

Figure 14. (a) Schematic illustration of the synthesis procedure for PPy PsNMs using hydrated crystals of sodium decylsulfonate. (b) TEM image of PPy FsNM, a magnified image of the circle being displayed in (c). Reproduced with permission.[150] Copyright 2011, Elsevier.

Figure 15. Schematic representation of the main steps of fabrication and release for obtaining PEDOT/PSS nanofilms by a Supporting Layer technique. (a) Si substrate; (b) spin-coating deposition of the PDMS substrate layer; (c) spin-coating deposition of the PEDOT/PSS nanofilm; (d) casting of a thick PVA supporting layer; (e) cutting and (f) peeling of the bilayer (PVA supporting layer + PEDOT/PSS nanofilm); (g) freestanding PEDOT/PSS nanofilm floating in water after dissolving PVA. Reproduced with permission.[155] Copyright 2011, The Royal Society of Chemistry.

Figure 16. Schematic representation of the nanofilm structure made up of PEDOT-rich particles (orange) surrounded by the PSS matrix. The suggested percolative mechanism in nanofilms as thickness increases is depicted; length of conductive pathways between neighbor PEDOT particles (dashed red line) increase with thickness up to a percolation threshold, when multiple parallel pathways become available.

Figure 17. (a) Low (top) and high (bottom) resolution SEM micrographs of P3TMA powder. (b) Low resolution SEM micrograph of P3TMA nanosheet.

Figure 18. (a) SEM micrographs of hydrolytically degraded PE44-P3TMA FsNM (blend prepared using a 50:50 molar ratio) after 4 weeks (left) and 8 weeks (right) of immersion in PBS. Circles show the conductive phase (spherical aggregates of P3TMA). (b) Plot of the weight loss (%) versus the degradation time (days) in hydrolytic (filled symbols) and enzymatic media (empty symbols) for PE44 (triangles) and PE44-P3TMA (squares) films. (c) SEM micrographs of Cos-7 and Du-145 cells adhered on the surface of PE44-P3TMA nanomembranes. The film surface (domains without cells) is shown by asterisks (*), while the connections or interactions between the cell and the surface or between two cells are indicated by arrows.

Figure 19. (a) Digital camera image of a PE44-P3TMA FsNM immersed in ethanol; (b-c) aspiration of the nanomembrane floating in ethanol into a pipette; (d-e) release of the folded nanomembrane into the ethanol solution; and (f) aspect of the nanomembrane after recovering the shape.

Figure 20. C-AFM characterization for TPU-P3TMA (40:60) nanomembrane deposited onto ITO: (a) Simultaneous 1 μm × 1 μm topographical image (left) and C-AFM current image (right) for the same sample. (b) Dual cross-section profile of above images indicating variations in height (solid line) and current (dashed line). (c) Typical current-voltage curves (100 nA/div amplifier, max top current 1 μA).

Figure 21. Weight loss of pure TPU and TPU-P3TMA (20:80, 40:60, and 60:40 ratios) films immersed in (a) PBS solution and (b) lipase-containing PBS solution. Dashed lines were added manually to help following data progression. Relative cellular adhesion (c) and viability (d) on TPU, P3TMA, and TPU-P3TMA (20:80, 40:60, and 60:40 ratios) nanomembranes. Assays were carried out using the following cell lines: Vero (dashed bars) and Cos-7 (empty bars). The relative viability was established in relation to the TCP control (tissue culture polystyrene). Steel was also considered as a control substrate because the individual polymers and the blends were deposited on this material. Greek letters on the columns refer to significant differences ($p < 0.05$) using the ANOVA and Tukey test: α vs TCPS; β vs steel.

Figure 22. SEM-AFM images of TPU-P3TMA/collagen nanomembranes: (a) height image 5 × 5 μm2; (b) cross sectional data from (a); (c) height image 1×1 μm^2; (d) phase image 1×1 μm^2 of (c); (e and f) SEM images (14 k× and 150 k×, respectively). Reproduced with permission.[171] Copyright 2014, American Chemical Society.

Figure 23. Scheme of a bilayered artificial muscle device made of ECP adhered to a non-conductive tape. Clockwise and anticlockwise movements are schematically represented by bended dashed lines at left and right, respectively.

Table 1. Comparison of the chemical and electrochemical polymerization processes for the preparation of ECP.

Polymerization Method	Advantages	Disadvantages
Chemical	- Large-scale production - Ease post-incorporation of other molecules to modify the ECP covalently - Many options to modify the chemical structure	- The synthetic process is more complicated than the electrochemical one - Preparation of ultra-thin films becomes a difficult task
Electrochemical	- Ease of synthesis - Entrapment of molecules in polymer network becomes an easy process - The synthetic and doping processes occur simultaneously - Very useful to prepare ultra-thin films of controlled thickness	- Removal of the films from the electrode surface is frequently a very difficult task. - Post-covalent modification of ECP is quite complex or, even, impossible

Table 2. Summary of the most important characteristics (*i.e.* preparation method, thickness, properties and potential biomedical applications) of FsNM made of insulating and electrochemically inactive polymers.

Material	Preparation	Thickness (nm)	Properties [a]	Biomedical applications	Ref.
PLA	Spin-coating	23±5	E: 1.7±0.1 GPa, L_c= (1.7±0.3–1.8±0.2)·10^{-5} N/m. Transparency	Wound dressing, atraumatic fixation tool	56-58
PLA	Spin-coating assisted multilayering	60±6	Transparency	Barrier against burn wound infection	59
PLA	Spin-coating	320±27	E: 136±44 MPa. Transparency	Patch for bone or tendon repair and healing, adhesive bioactive matrix for cell anchoring, spreading and proliferation	60,61
PLA-mesh	Spin-coating with the nanosheet collected on a stainless steel mesh	From 29±1 to 703±4.4	E: from 3.5±1.3 to 7-10 GPa. Transparency. Weak adhesiveness for higher thickness nanosheets	Tailorable environment for anisotropic cell proliferation and differentiation without using conventional photolithographic approaches	62
PLA coated with collagen at one side	Spin-coating	59.5±9.5 (PLA) and 5-10 (collagen)	Weak adhesiveness	Scaffolds that endow each side of the nanosheet with different discrete functions: anti-adhesive and pro-healing	63
PLA + SPION	Spin-coating	From 33±3 to	E similar to PLA. Magnetically responsive and	Magnetically controllable support	64

		245±9	colored		
PLA / PAH-D / HA	Spin-coating + LbL	~500 nm	Robust and flexible	Drug delivery	65
PLGA	Thermal fusion of adsorbed nanoparticles	-	-	Platelet substitute, carrier	66
Chitosan / Na-alginate	Spin-coating assisted LbL	From 30.2±4.3 to ~75	E= 1.3 / 9.6 GPa. Pressure resistance, high flexibility and adhesiveness, transparency, biodegradability and semi-absorbent ability	Nano-adhesive plaster for tissue surfaces. Tissue defect repair without chemical bonding agents. Multi-overlapping therapy for venous hemorrhage. Arachnoid plaster in microsurgery without using chemical bonding agents.	68-71, 74, 75
PVA / TC / (chitosan / Na-alginate)	Spin-coating assisted LbL	177	High flexibility, adhesive strength and transparency	Overlapping therapy, treatment of burn wound infections, antimicrobial platforms and drug-loading	72, 73
HA / collagen	LbL	42±4 (fibrous collagen) and 62±7 (non-fibrous collagen)	For fibrous collagen: E= 12.5±1.5 GPa, σ_{max}= 289±9 MPa and ε_{max}= 1.0±0.1%. For non-fibrous collagen: E= 4.3±0.6 GPa, σ_{max}= 227±10 MPa and ε_{max}= 1.7±0.3%	Scaffolds for regenerative medicine	76
Cell / gelatin / (chitosan / Na-alginate)$_3$	LbL onto cultured cells on PNIPAM-grafted surfaces	-	-	Fabrication of complex artificial soft tissues to substitute some elements of native tissues	78
PEO / PAA	LbL	80 nm per bilayer	Elastomeric properties, smooth to the touch and	Biosubstrates, drug delivery devices and pH-sensitive sensors	85

			transparent,		
PAA / PEG – PAH / PSS	Spraying polymer solutions	55 to several hundreds	Components biocompatible, biotolerated or bioinert. Transparent and pH responsive	Therapeutic devices and aids	86
NBPT-PEG	Spin-coating	~5	Mechanical stability, biocompatibility and high transparency. Protein-repelling behavior	Support in transmission electron microscopy studies in their specific application to sensitive biological targets	87
PEG	Chemical crosslinking of a hydrogel precursor	10-350	Mechanical stability, high flexibility (E= ~ 2MPa), hydrophylicity, biorepulsion	Highly sensitive support and sensor element for biological samples	88
PAH / PAA	LbL dipping + pH treatment for the creation of pores	253-688	Pores with diameters ranging from 300 nm to 2 μm (average: 1 μm)	Drug-delivery systems tuned by varying the number of layers and the pore size.	11
PDDA / P4VPPS	LbL	~29 per bilayer	pH-dependence, disintegrating in alkali environments	Support (sacrificial layer) for biological templates	92
PHEMA	Surface-initiated ATRP on a PDA layer	16-75	Good chemical stability, low mechanical strength, transparency and colorless	Multi-stimuli responsive sensors after functionalizing the surface of the films	94
PMPC / (PS, PAH, PAA)	ATRP of MPC and spin-coating assisted LbL	11 (PMPC) + 85±2 (PS, PAH, PAA)	Physiological stability, surface wettability and anti-biofouling	Biointerface for tissue-engineering scaffolds	95
PMMA	Spin-coating	199±20	High flexibility, physiological stability and expected	Fabrication of platforms with space-selective cell culture environments by	96

			mechanical behavior similar to that of PLA FsNM	injet printing protein microarrays at the surface. Cell-directed culture in muscular tissue engineering	
PMMA	Spin-coating PMMA:PS mixtures	From 38.8±1.1 to 110.2±2.0 nm	Porous and perforated structures	Potential application in cell culture devices, high flux biosensors and drug delivery systems	97
PS – (CNT-Fn)	Spin-coating (PS) with microcontact printing (CNT-Fn)	From tens (~40) to hundreds (~360)	High flexibility, cell adhesiveness and surfaces with tailored morphology	Platforms to direct the cellular organization and engineer the hierarchically assembled tissue structure. Flexible devices for regenerative medicine	98
$(PAH/PSS)_nPAH$-Au-$(PAH/PSS)_n$-PAH	Spin-coating assisted LbL	25-70	E= 30-40 GPa, σ_{max}> 100 MPa and ε_{max}= 2%. Light blue color. Long life, extraordinary sensitivity and unique auto-recovering ability	Although no biomedical application was directly examine, these FsNM are potential candidates for their use in systems requiring outstanding mechanical and dynamical properties.	4, 99
PAA / DMLPEI	LbL	< 100 (from 2 to 20 bilayers)	Mechanical robustness, pH responsive	Coatings with microbicide properties for airborne and waterborne bacteria	101
DGI	Free-radical polymerization under UV radiation	< 5	High mechanical strength and thermal stability. High-density of functional groups exposed to the outer surfaces	Practical applications in the biomedical field depend on the surface post-functionalization	104

[a] E: Elastic modulus. L_c: Critical load related to the adhesion. σ_{max}: Ultimate tensile strength. ε_{max}: Ultimate tensile elongation.

Table 3. Summary of the most important characteristics (*i.e.* preparation method, thickness, properties and potential biomedical applications) of FsNM made of ECP and electrochemically inactive polymers.

Material	Preparation	Thickness (nm)	Properties [a]	Biomedical applications	Reference
PPy	Interface polymerization	From 60 to hundreds	σ= 1.14 S/cm for a thickness of 230 nm. Flexible, transparent, shiny and light-blue color.	Those in which films with different roughness and water wettability on each side of film fit	149
PPy	Organic crystal surface-induced polymerization	~21	σ= 30.6 S/cm. Smooth surface	Chemical sensor, successful results being obtained with HCl and NH_3 vapors	150
PPy	*In situ* FIP	~100	Extremely high electrical conductivity with σ= 2000 S/cm. Semi-transparency and smooth surface	Fabrication of sensors	151
PPy	Interface polymerization using porphyrin as *in situ* template	From 50 to 250	Low conductivity ($\sigma \approx 10^{-5}$ S/cm) that can be adjusted by doping. Mechanically strong and dense morphology	Biosensors and artificial muscles	152
PEDOT / PSS	Supporting Layer	From ~40 to ~100	Conductivity, σ= 0.88-1.44 S/cm) comparable to that of micrometric films (σ= 1.38 S/cm). E= 0.81-1.02 GPa.	Bioactive platforms. Electrochemical soft microactuators (microfingers) for cell manipulation with microrobots	155,158

			Flexibility.		
PEDOT / PSS	Spin-coating +heat-shrinking process	From 53.6±1.2 to 120.9±1.5	R= 199±11 - 586±16 Ω per square Presence of anisotropic topographical cues at the micro- and nanoscale on the surface	Smart scaffolds for functional cell alignment and electrical stimulation.	160
PEDOT-carbon nanotube sheet	Vapor phase polymerization	~66	R= 200 Ω per square. E= 12.6 GPa, σ_{max}= 135 MPa. Volumetric capacitance: ~40 F/cm^3 at 100 V/s. Flexibility and transparency.	Sensors and actuators	162
PE44-P3TMA	Spin-coating	From 20 to 80	σ= 10^{-4} to 10^{-5} S/cm depending on the composition of the blend. Robustness, flexibility and transparency. Yellowish color. Biodegradable and electro-compatible with cells.	Bioactive platforms with semiconducting response for tissue regeneration.	167,168
TPU-P3TMA	Spin-coating	From 11 to 93	σ= from $2.23\cdot10^{-5}$ to $5.19\cdot10^{-6}$ S/cm, current= from 0.43 to 1.85 pA. E= 0.9-1.7 GPa, $F_{adh}\approx$ 6 nN. ε_g= 2.35 eV. Robustness, flexibility and transparency. Yellowish color. Biodegradable and electro-compatible with cells.	Bioactive substrates for advanced biomedical applications	169-171
(PEDOT/PSS) / PLA	Spin-coating	~45 (PEDOT/PSS	σ= 180 S/cm. Mechanical robustness and	Smart conductive biointerfaces for directing cell adhesion and	172

		layer) + ~200 (PLA layer)	conformability. Colors from dark blue to light blue or even transparent depending on the oxidation state. Electrochemical regulation of the surface wettability.	differentiation. Bioelectrodes.	
(TPU-P3TMA) / collagen	Spin-coating + adsorption	From 11 to 93 (TPU-P3TMA layer) + 73 (collagen layer)	Formation of a pseudoregular honeycomb 2D network, in which the top layer resembled a fibril structure	Three-dimensional scaffolds for tissue engineering	171

[a] σ: Electrical conductivity. R: Electrical resistance. E: Elastic modulus. σ_{max}: Ultimate tensile strength. F_{adh}: Adhesion force between the AFM tip and the sample surface. ε_g: Optical band gap energy.

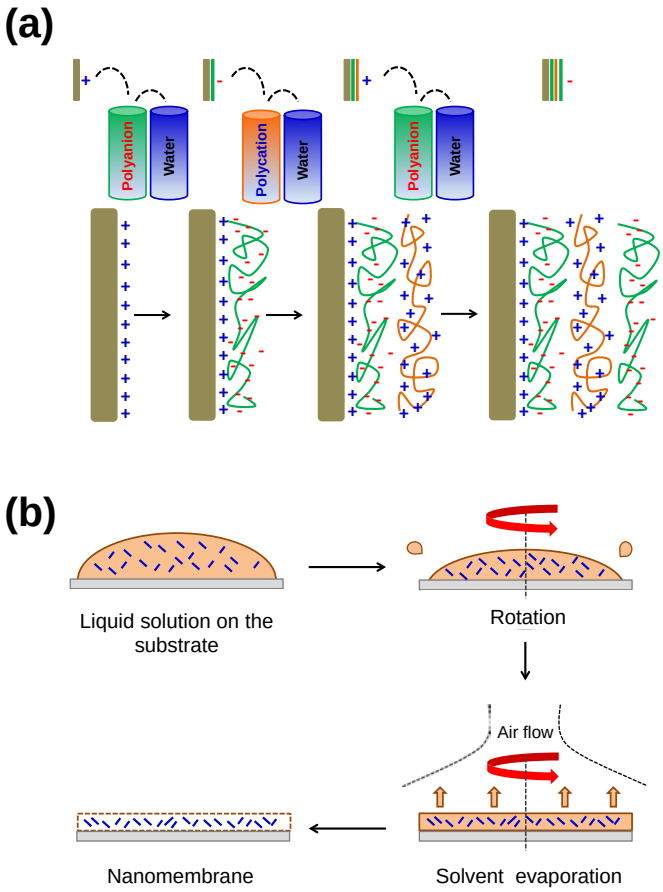

Figure 1

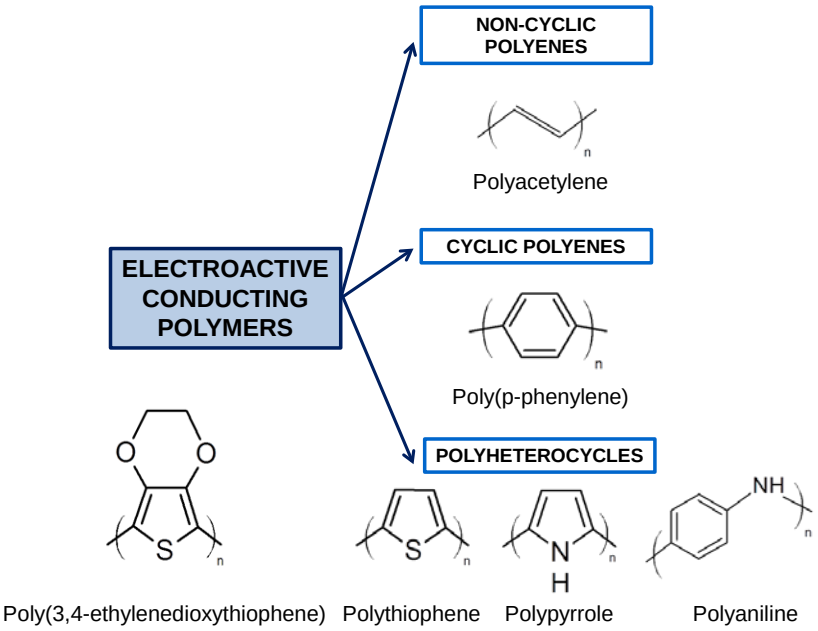

Figure 2

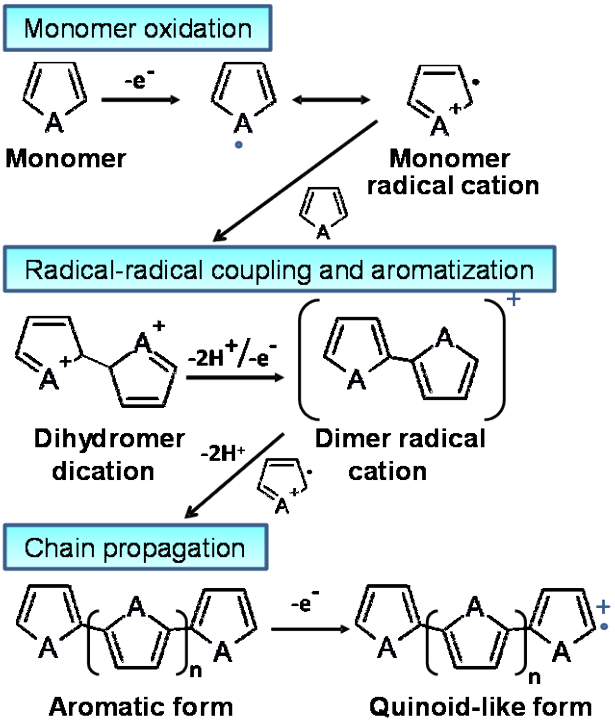

Figure 3

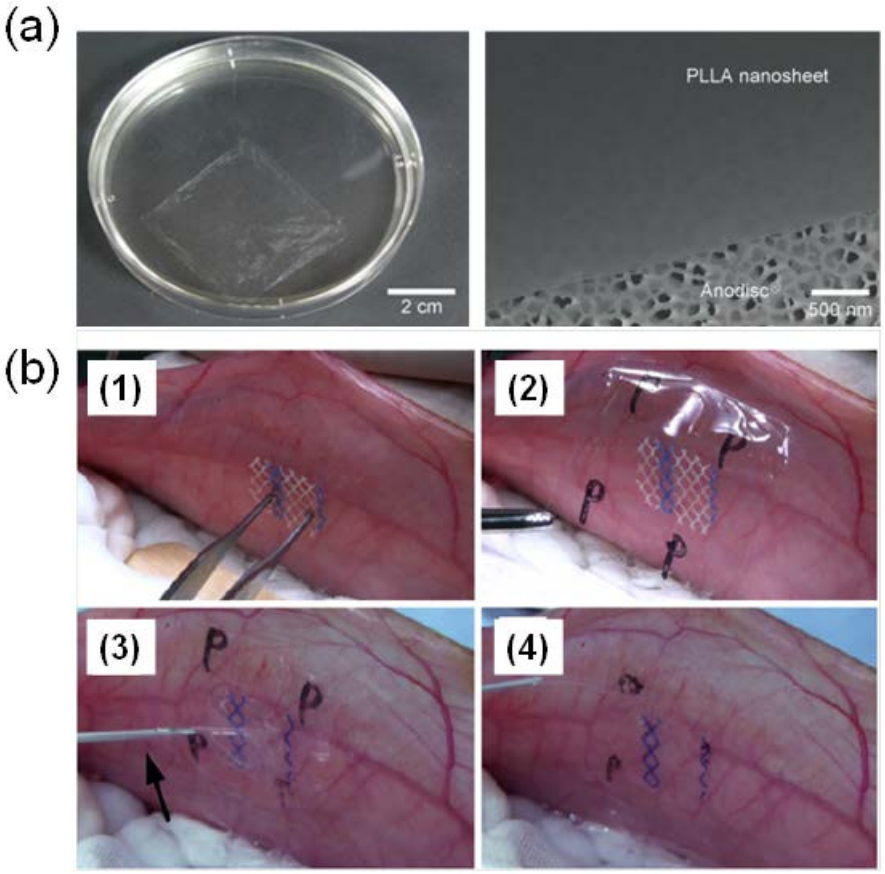

Figure 4

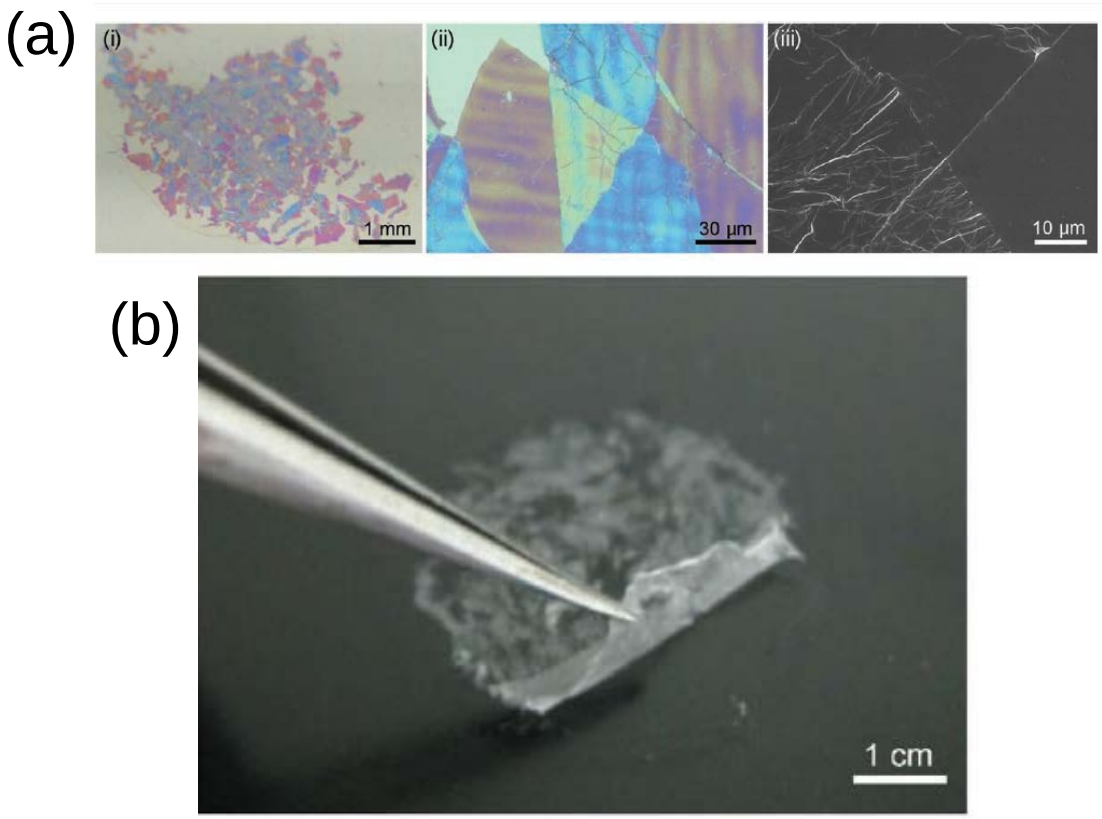

Figure 5

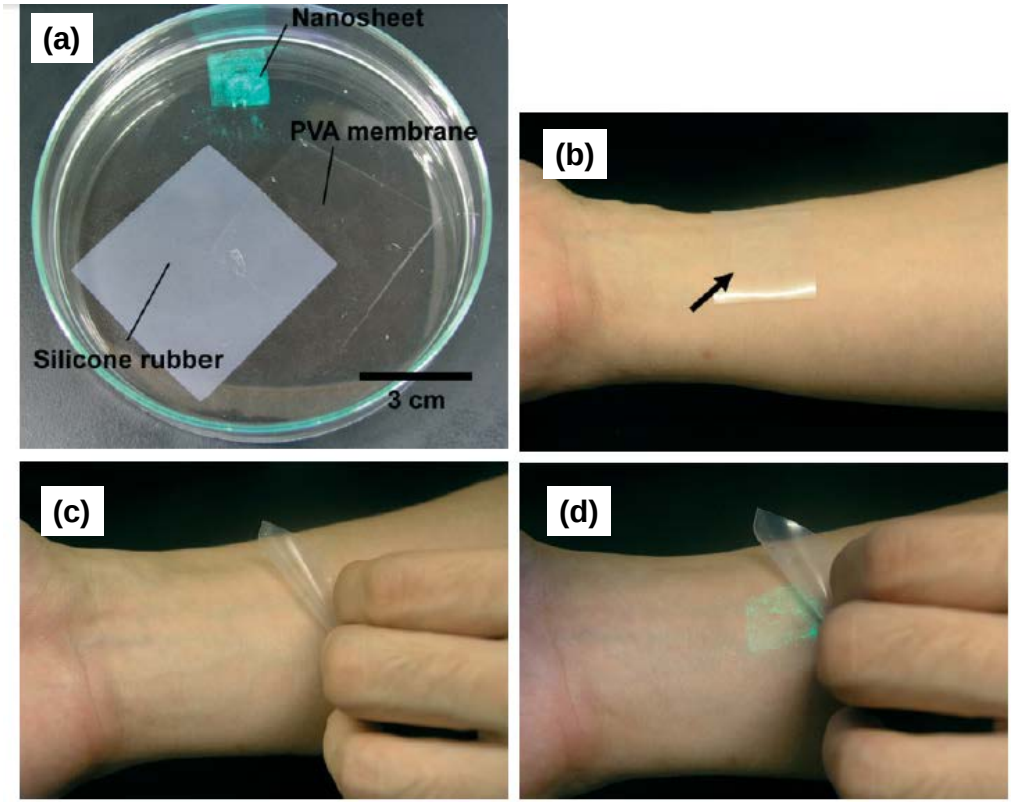

Figure 6

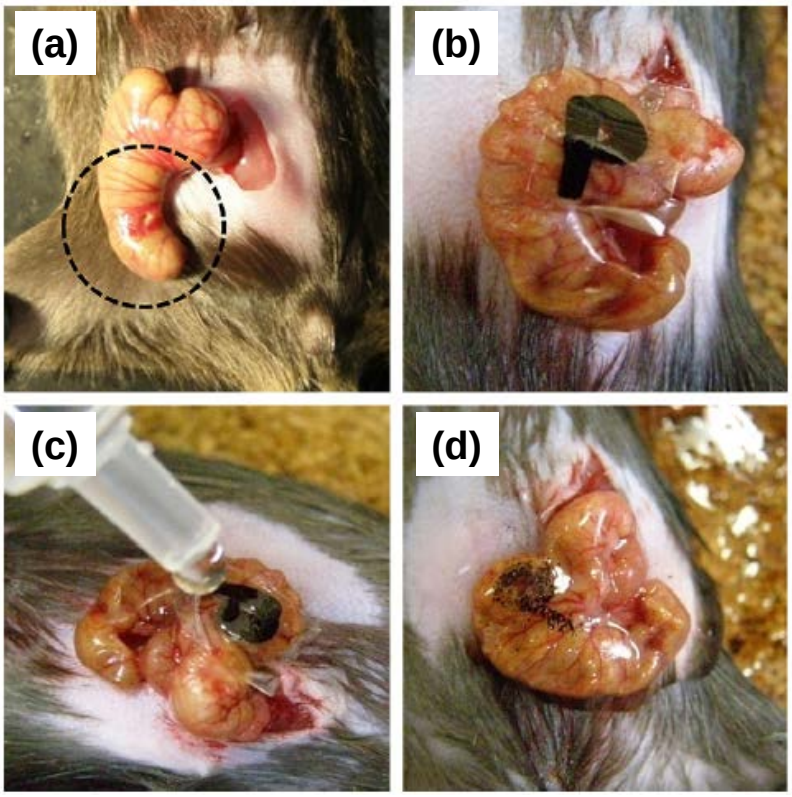

Figure 7

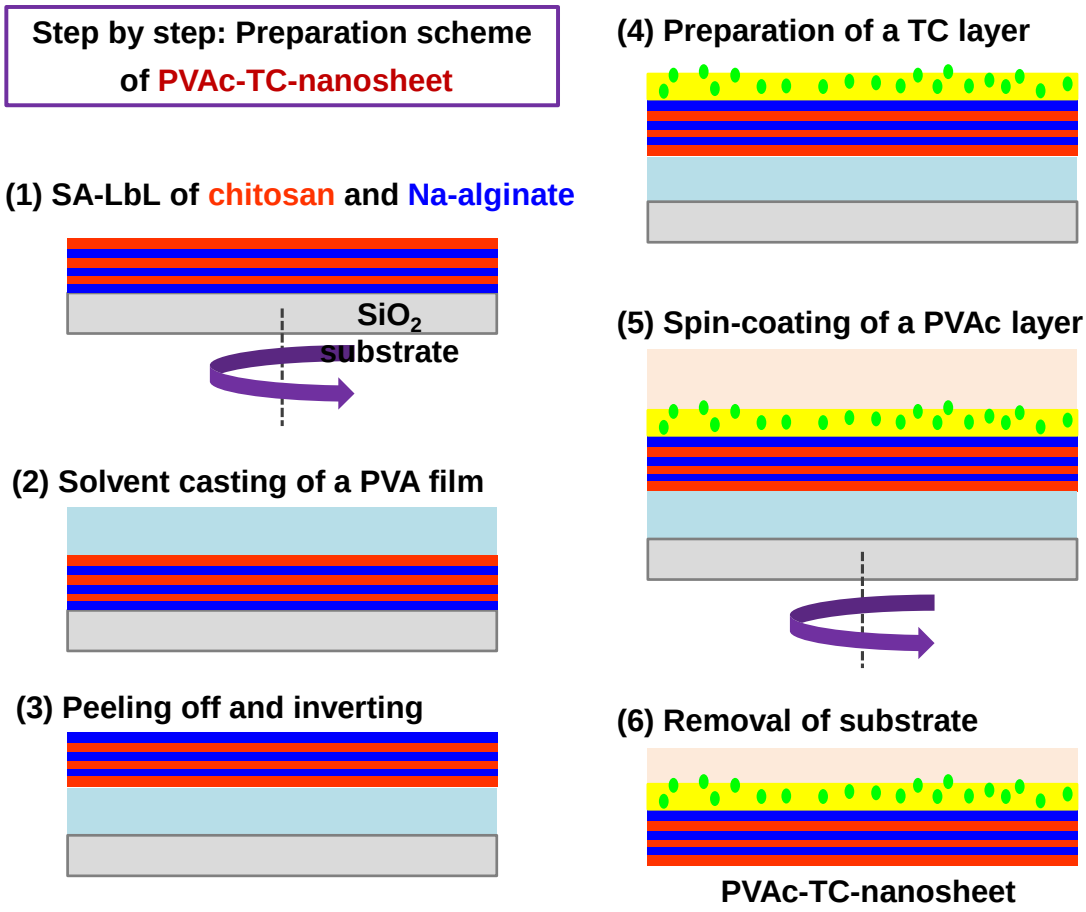

Figure 8

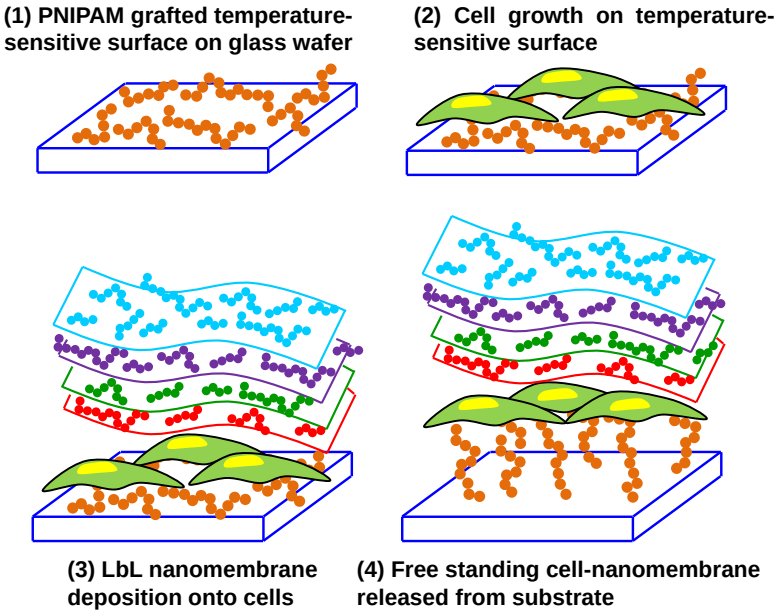

Figure 9

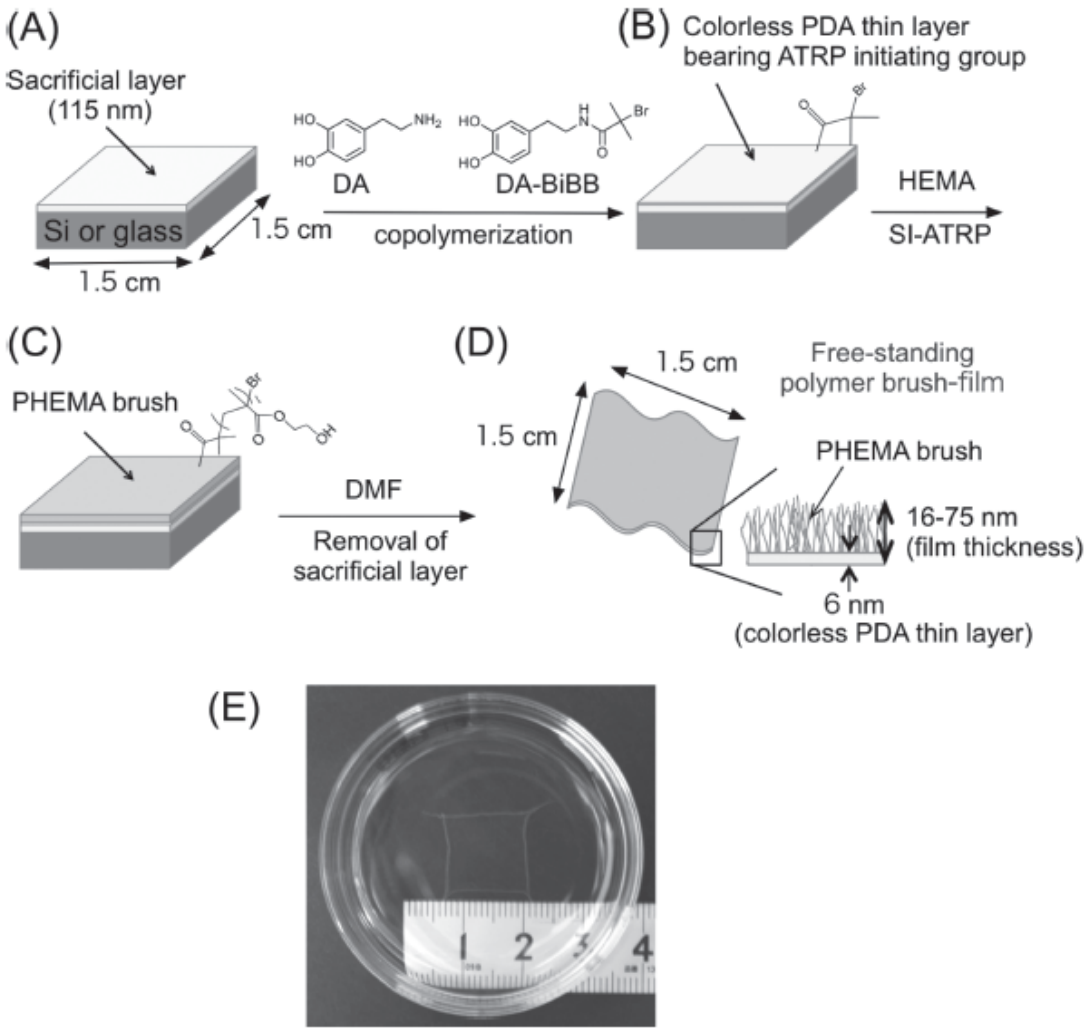

Figure 10

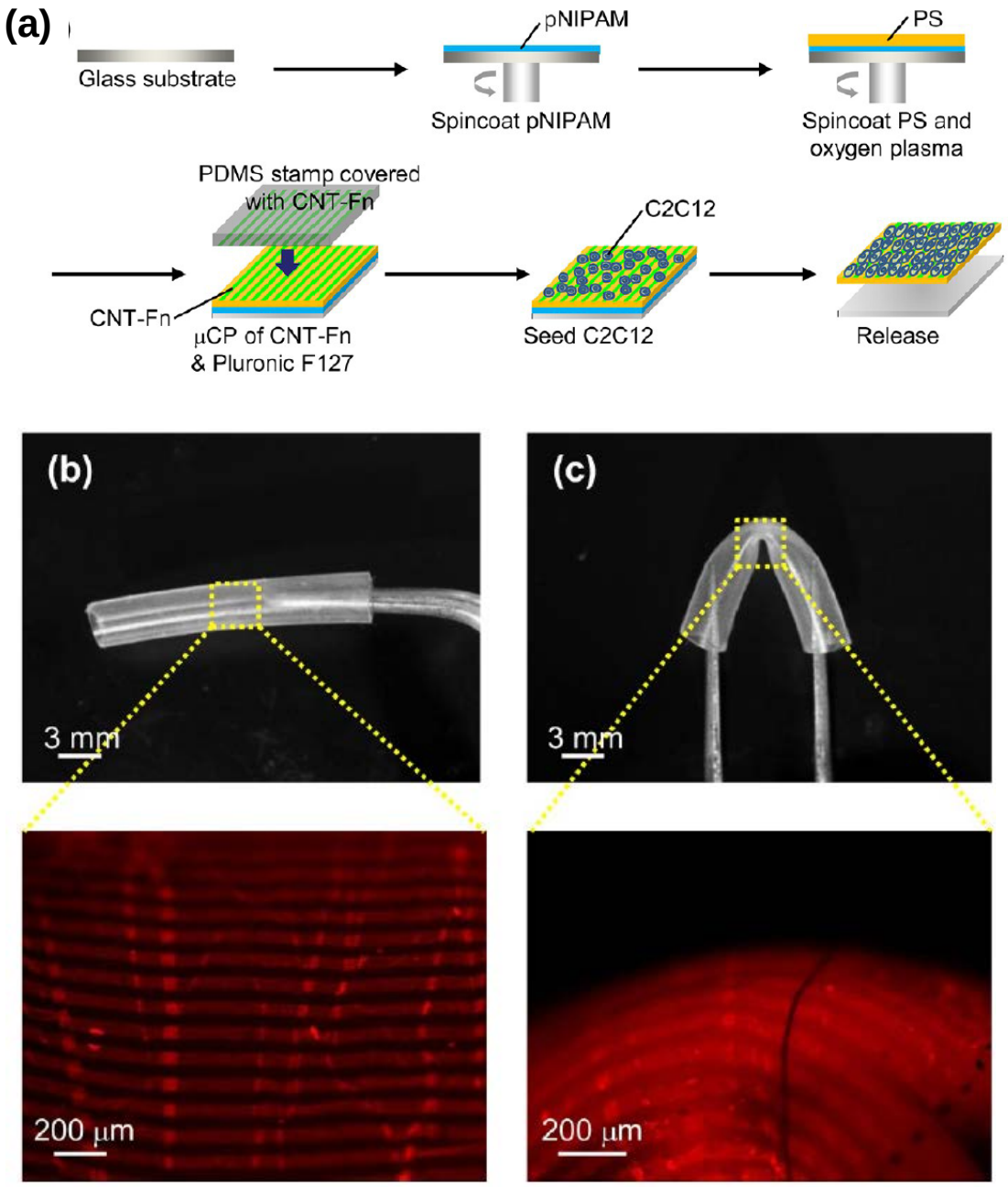

Figure 11

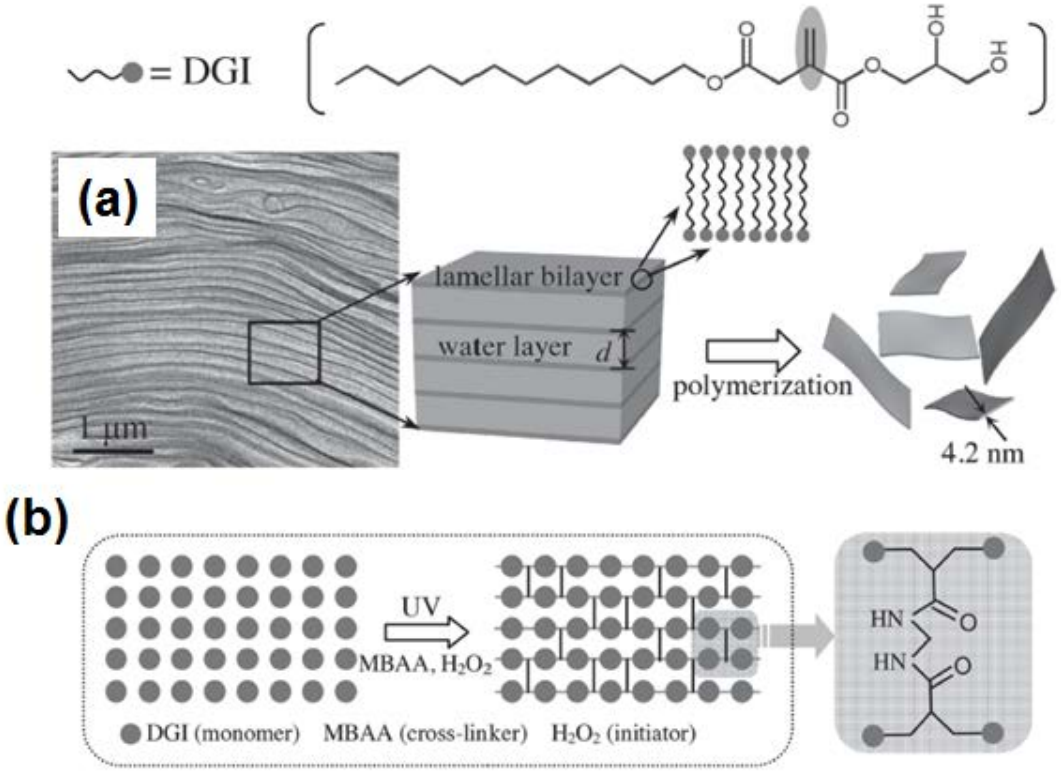

Figure 12

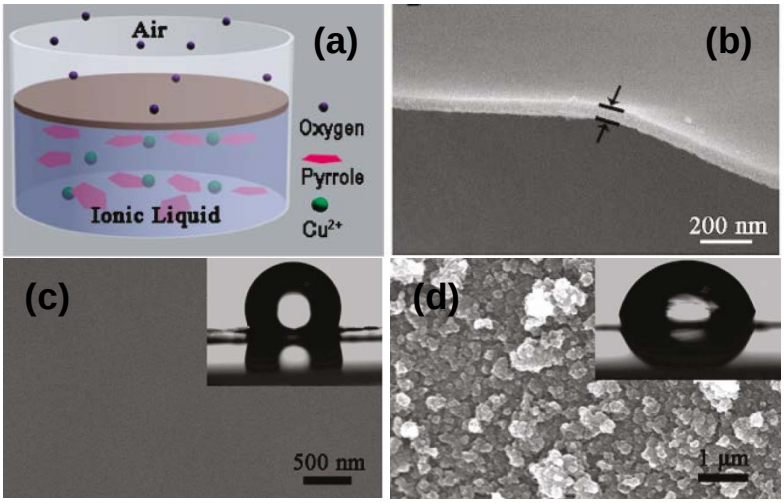

Figure 13

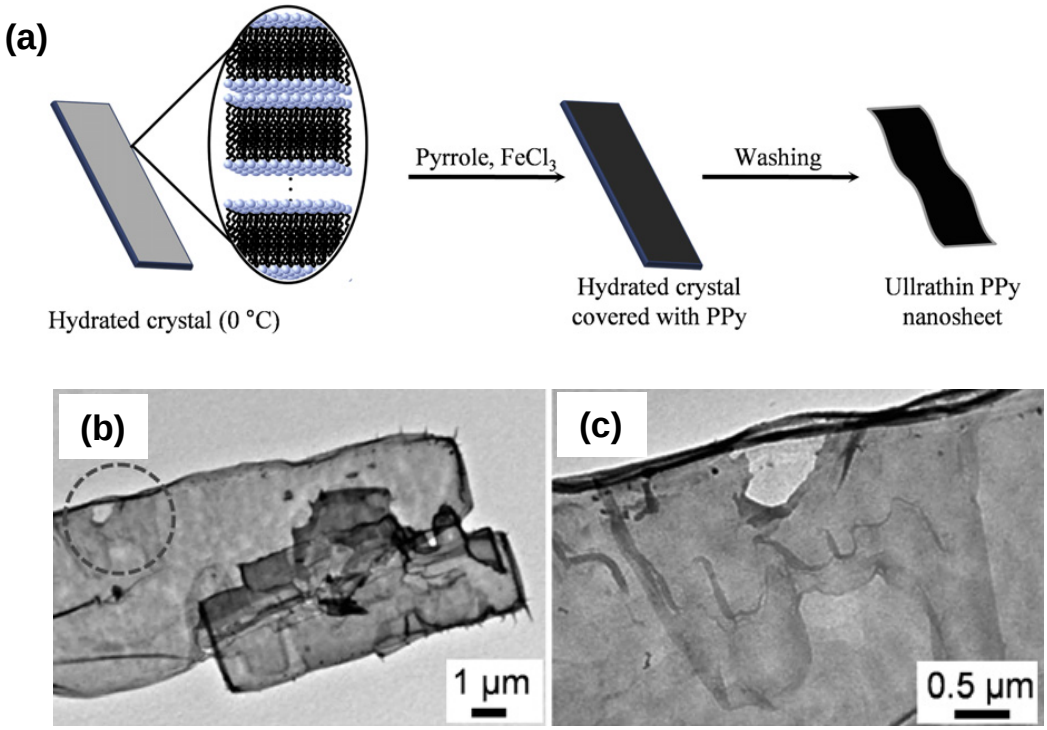

Figure 14

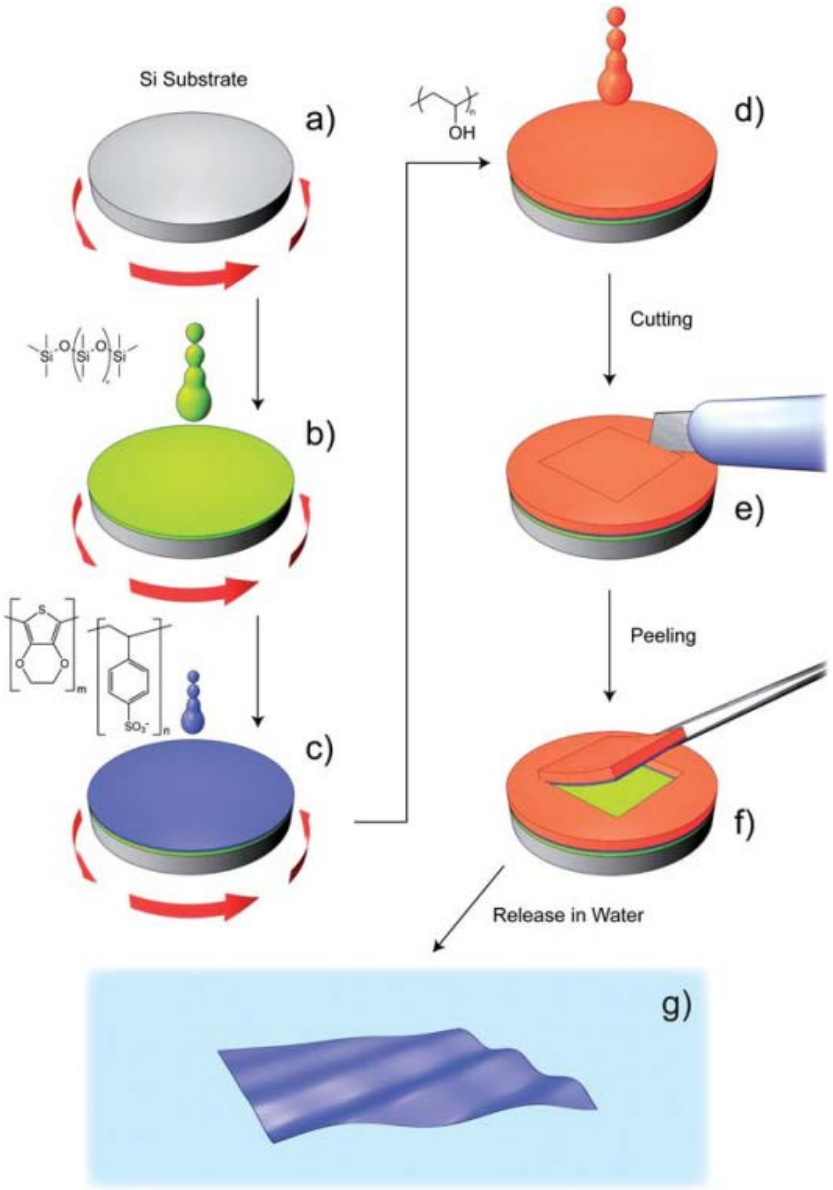

Figure 15

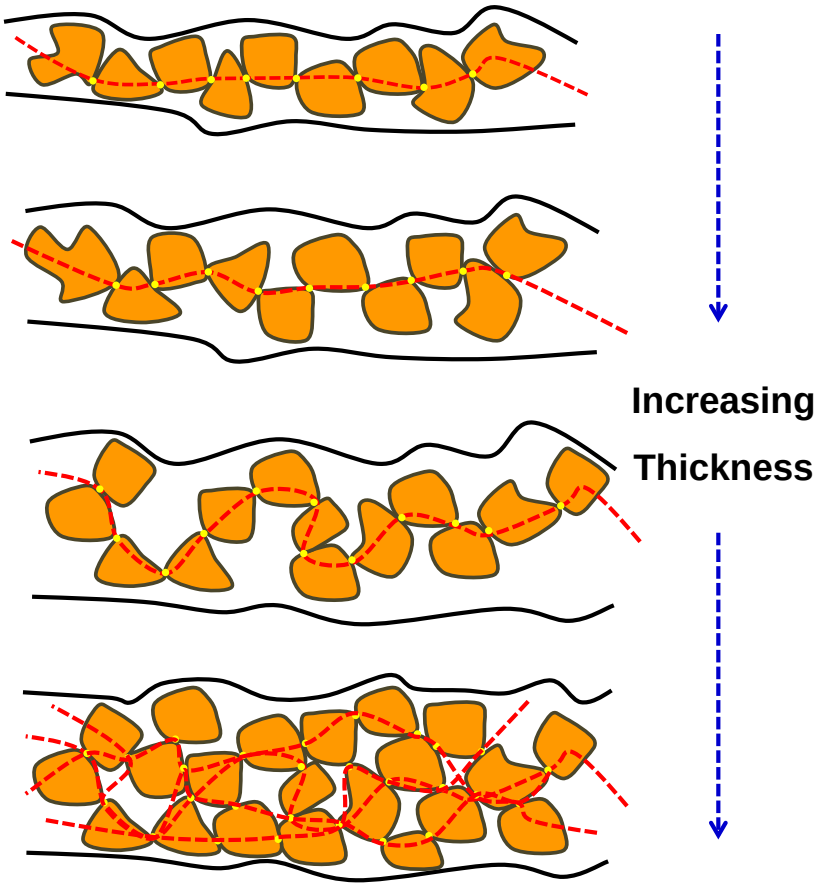

Figure 16

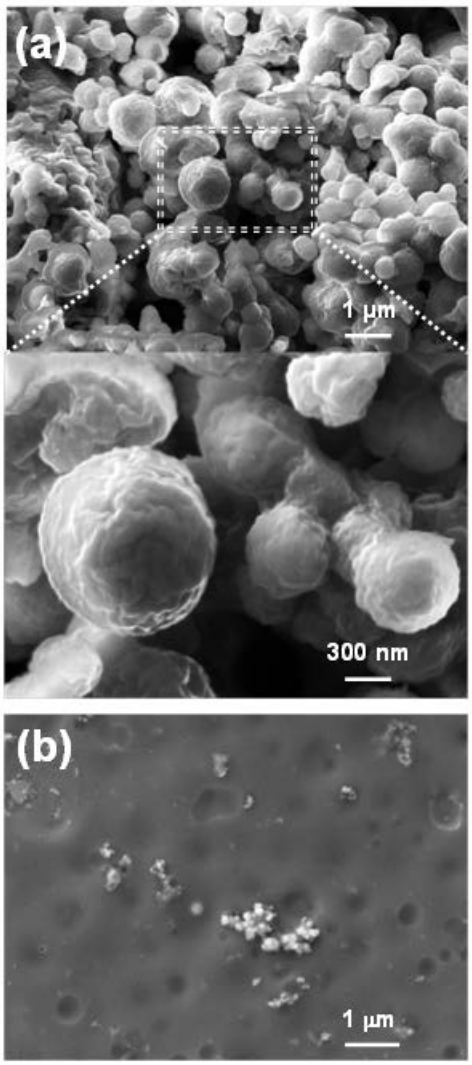

Figure 17

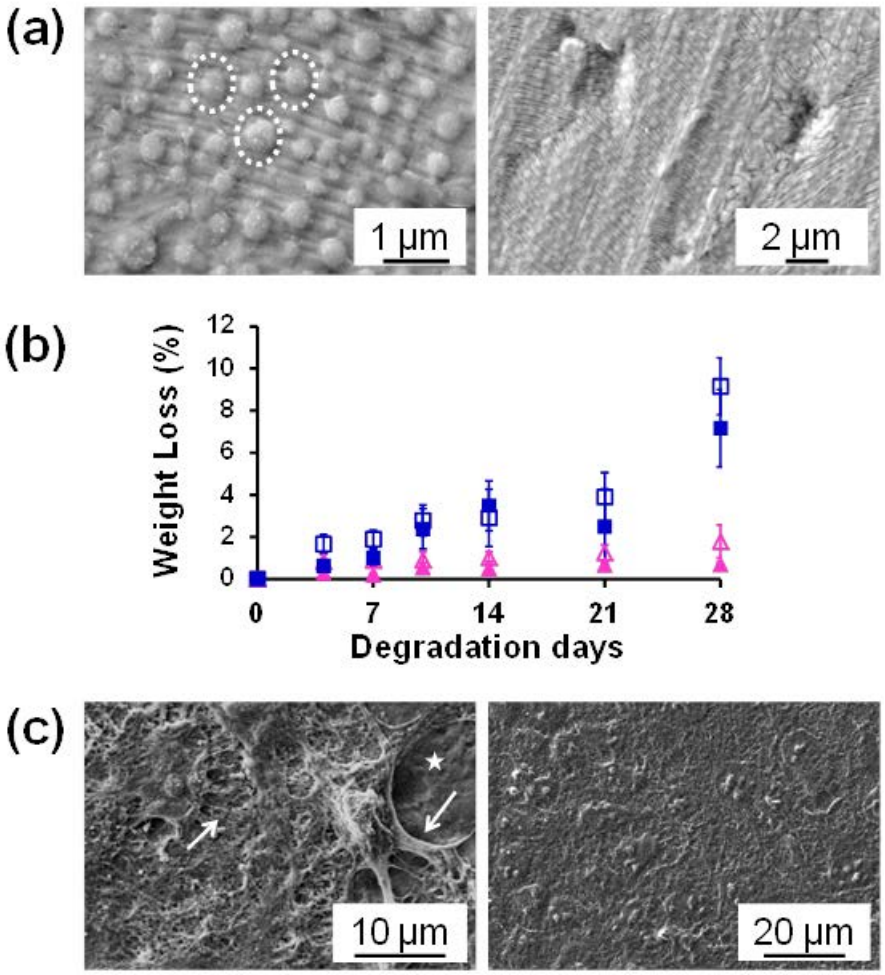

Figure 18

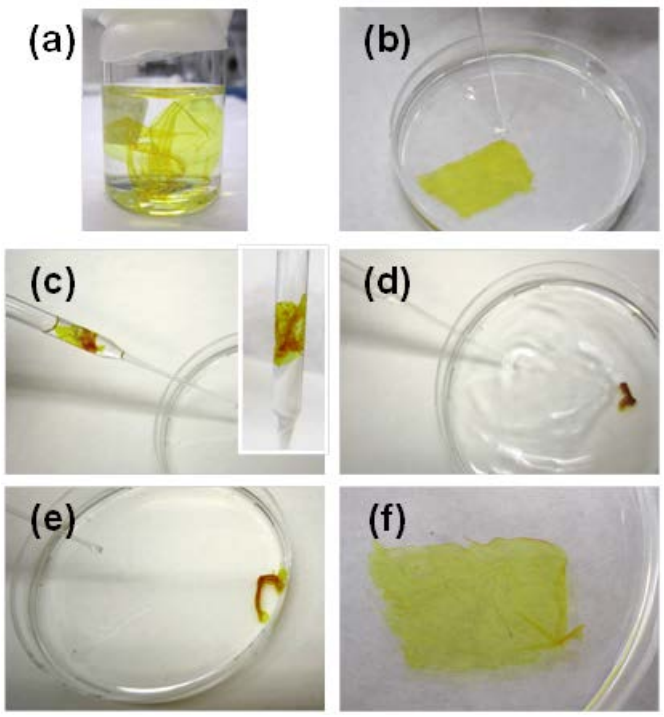

Figure 19

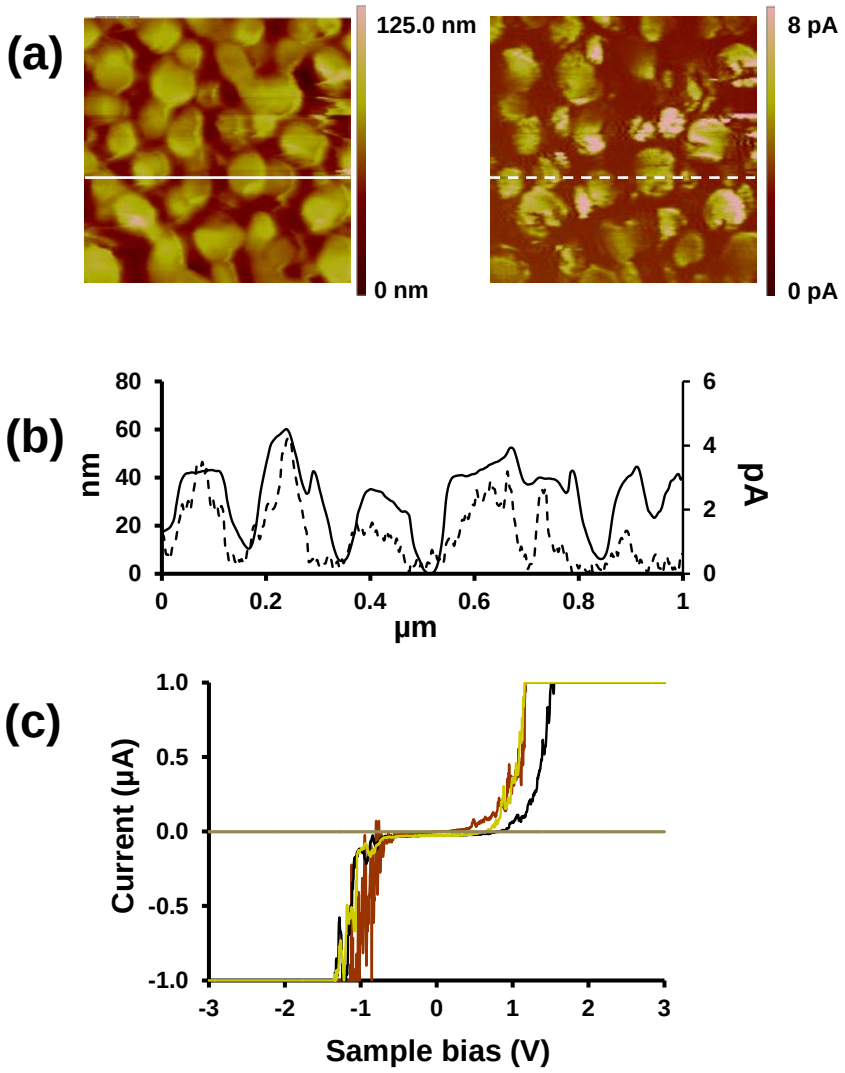

Figure 20

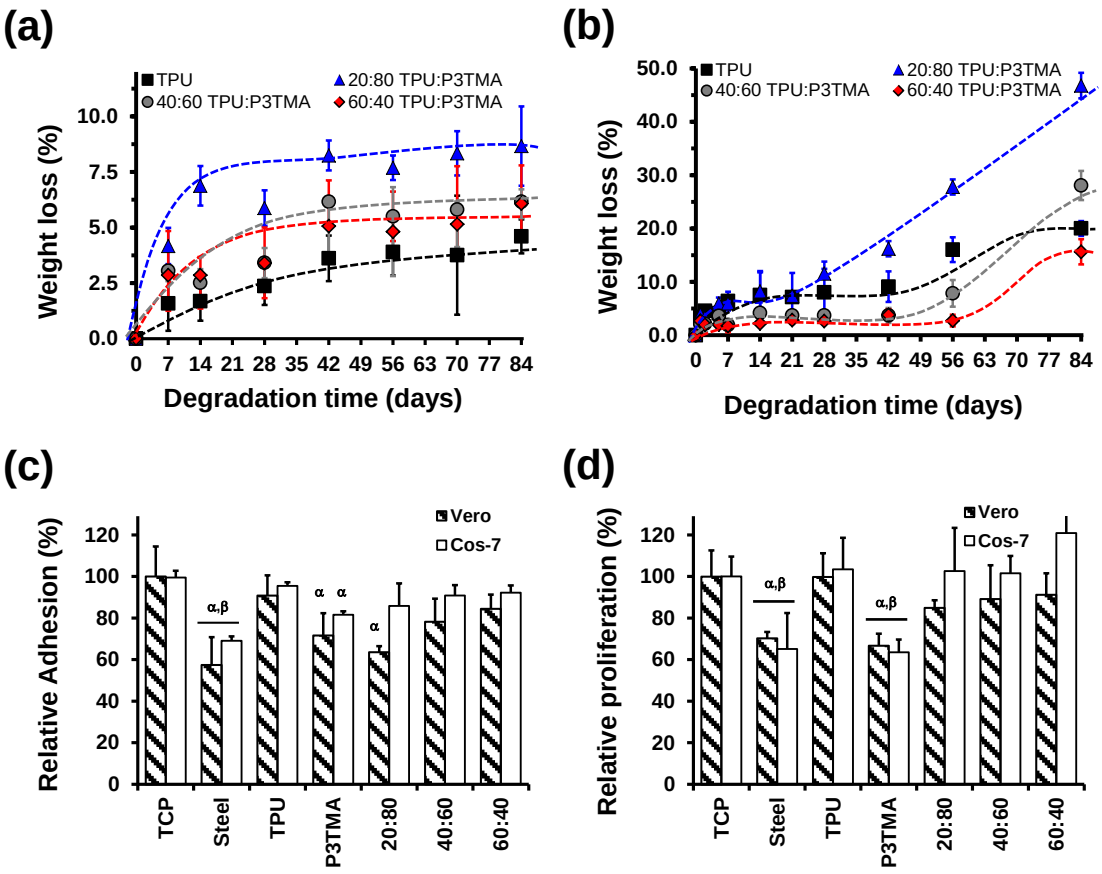

Figure 21

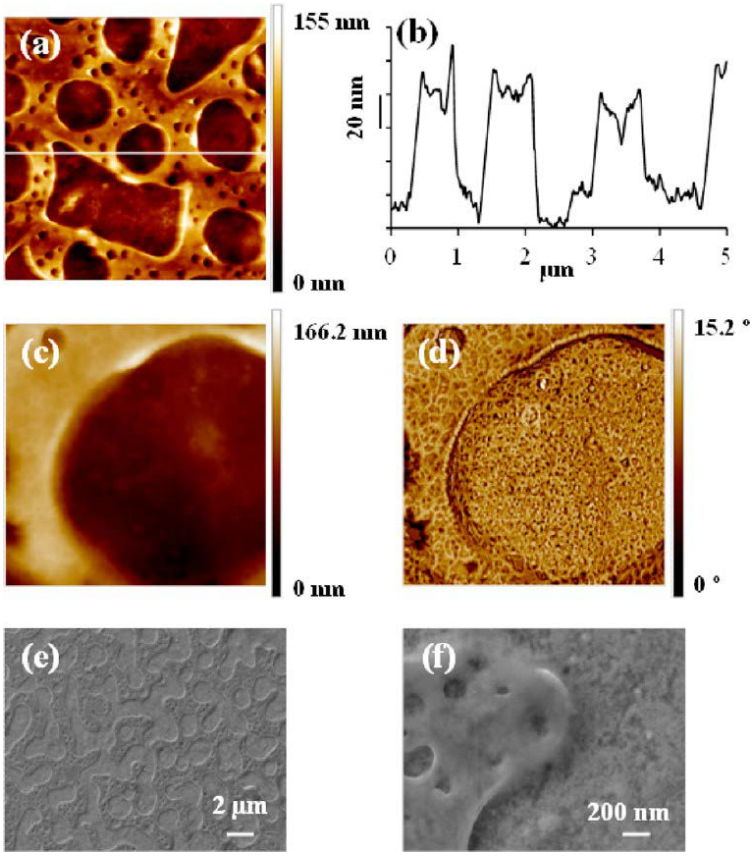

Figure 22

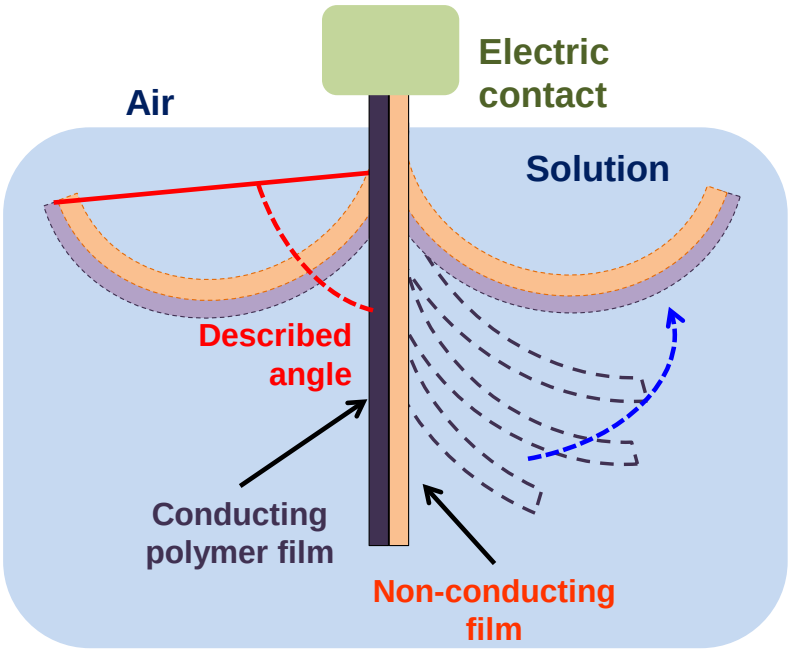

Figure 23

Free-standing nanomembranes, which are emerging as versatile elements in biomedical applications, are evolving from being composed of insulating (bio)polymers to electroactive conducting polymers.